Quaternary Science Reviews xxx (2014) 1–17

Contents lists available at ScienceDirect

Quaternary Science Reviews

journal homepage: www.elsevier.com/locate/quascirev

Invited review

# Revisiting the Y-3 tephrostratigraphic marker: a new diagnostic glass geochemistry, age estimate, and details on its climatostratigraphical context

Paul G. Albert [a,b,*], Mark Hardiman [c,d], Jörg Keller [e], Emma L. Tomlinson [f,a], Victoria C. Smith [b], Anna J. Bourne [c,g], Sabine Wulf [h], Giovanni Zanchetta [i], Roberto Sulpizio [j], Ulrich C. Müller [k], Jörg Pross [k,l], Luisa Ottolini [m], Ian P. Matthews [c], Simon P.E. Blockley [c], Martin A. Menzies [a]

[a] Department of Earth Sciences, Royal Holloway University of London, Surrey TW20 0EX, United Kingdom
[b] Research Laboratory for Archaeology and the History of Art, Oxford University, Oxford OX1 3QY, United Kingdom
[c] Centre for Quaternary Research, Department of Geography, Royal Holloway University of London, Surrey TW20 0EX, United Kingdom
[d] Department of Geography, University of Portsmouth, PO1 2HE, United Kingdom
[e] Institute of Geosciences, Mineralogy and Geochemistry, Albert-Ludwigs-University Freiburg, Albertstraße 23b, 79104 Freiburg, Germany
[f] Department of Geology, Trinity College Dublin, College Green, Dublin 2, Ireland
[g] Department of Geography, Swansea University, Singleton Park, Swansea, SA2 8PP Wales, United Kingdom
[h] Helmholtz Centre Potsdam, German Research Centre for Geosciences, Section 5.2 – Climate Dynamics and Landscape Evolution, Telegrafenberg, 14473 Potsdam, Germany
[i] Dipartimento di Scienze della Terra, via S. Maria 53, 56126 Pisa, Italy
[j] Dipartimento di Scienze della Terra e Geoambientali, Universitá di Bari, via Orabona 4, 70125 Bari, Italy
[k] Biodiversity and Climate Research Centre, Senckenberganlage 25, 60325 Frankfurt, Germany
[l] Paleoenvironmental Dynamics Group, Institute of Earth Sciences, Heidelberg University, Im Neuenheimer Feld 234, 69120 Heidelberg, Germany
[m] Consiglio Nazionale delle Ricerche (CNR) – Istituto di Geoscienze e Georisorse (IGG), Unità di Pavia, I-27100 Pavia, Italy

ARTICLE INFO

*Article history:*
Received 13 February 2014
Accepted 1 April 2014
Available online xxx

*Keywords:*
Y-3 tephra
Ionian Sea
Mediterranean tephrochronology
Tenaghi Philippon
Stadial conditions
Bayesian age modelling

ABSTRACT

The 'Y-3' tephra is a crucial stratigraphic marker within the central Mediterranean region that falls close to the Marine Isotope Stage 3/2 transition and a cooling event proposed as a correlative of the North Atlantic Heinrich Stadial 3 (HS3). Consequently, this tephra offers great potential to assess any leads and lags in environmental responses to this abrupt climatic transition. New grain-specific glass analysis (EMPA and LA-ICP-MS) of the type locality Y-3 tephra recorded in the Ionian Sea confirms its origin from Campi Flegrei (CF) but reveals that it is compositionally different from the previously suggested proximal equivalent the VRa eruptive unit (Verdolino Valley, CF). Consequently, the $^{40}Ar/^{39}Ar$ age of the VRa should not be exported distally to the Y-3 tephra. Instead, we propose a new robust age for the Y-3 tephra following its identification in the Tenaghi Philippon sedimentary record, NE Greece. A Bayesian-based $^{14}C$ age model from Tenaghi Philippon provides a distal age of 28,680–29,420 cal yrs BP for the Y-3 tephra. The identification of this tephra in NE Greece markedly extends its known eastern dispersal. Whilst its stratigraphic position falls within the latter part of a period of low tree pollen percentages related to dry stadial conditions. This new age and environmental context suggest that this marker postdates the onset of HS3 in the eastern Mediterranean region by ~2300 years.



## 1. Introduction

Northern hemisphere palaeoenvironmental archives indicate that the Last Glacial period was punctuated by abrupt and high-amplitude climatic variability (Dansgaard et al., 1993; NGRIP Members, 2004; Rasmussen et al., 2006), a variability that is observed in Mediterranean climate archives (Allen et al., 1999;

* Corresponding author. Research Laboratory for Archaeology and the History of Art, Oxford University, Oxford OX1 3QY, United Kingdom. Tel.: +44 01865 285225.
*E-mail address:* paul.albert@rlaha.ox.ac.uk (P.G. Albert).

http://dx.doi.org/10.1016/j.quascirev.2014.04.002
0277-3791/

Sanchez Goñi et al., 2000; Tzedakis et al., 2002, 2004; Kotthoff et al., 2011; Müller et al., 2011). However detailed assessment of the spatial and temporal patterning of this extreme climate variability, even at a centennial resolution, is limited by the precision and accuracy of the available chronological information. Radiocarbon dating ($^{14}C$) remains the most frequently adopted geochronological tool for the last 50 ka BP, but its precision is often insufficient to assess the exact timing of climatic change between different archives and is further complicated by inherent uncertainties associated with temporal variations in marine reservoir offsets (Siani et al., 2001).

Volcanic ash (<2 mm) or tephra associated with explosive volcanism can be used to synchronise palaeoenvironmental archives (i.e. tephrostratigraphy) owing to its widespread and synchronous deposition. Furthermore, where the age of a tephra can be determined it provides a chronological marker (i.e., tephrochronology). The high frequency of explosive volcanic activity in the Mediterranean region during the Late Quaternary has made tephra layers particularly powerful chronological tools with marine (e.g., Keller et al., 1978; Vinci, 1985; Paterne et al., 1986, 1988, 2008; Vezzoli, 1991; Calanchi et al., 1998; Hardiman, 1999; Aksu et al., 2008; Albert et al., 2012) and terrestrial (e.g., Ramrath et al., 1999; Wulf et al., 2004, 2008; Margari et al., 2007; Wagner et al., 2008; Sulpizio et al., 2010; Vogel et al., 2010) archives. More recent cryptotephra (non-visible) studies have increased the geographic range of many known tephra markers and have also presented a number of new isochrons (Siani et al., 2004; Lowe et al., 2007; Bourne et al., 2010; Damaschke et al., 2013).

One of these layers crucial to the central Mediterranean tephrostratigraphy is the 'Y-3' tephra, a tephra first identified and labelled based on its occurrence in the Last Glacial (climate zone Y) marine sediments of the Ionian Sea (Keller et al., 1978) (Fig. 1a). This K-trachytic tephra was reported stratigraphically above the thicker K-trachytic Y-5 layer and was thought to be associated with major explosive activity from the Campanian region (Keller et al., 1978). The presence of the Y-3 tephra was later confirmed in new Ionian Sea sediment cores from the *Meteor* cruise M25/4 (Keller et al., 1996; Kraml, 1997) (Fig. 1a). The Ionian Sea records can therefore be considered the 'type locality' for the Y-3 distal marker tephra. The thickness of this K-trachytic ash layer in the Ionian Sea records (Table 1), over 450 km from Campanian Volcanic Zone (CVZ) (Table 1; Fig. 1a), clearly demonstrates the large magnitude of this Campanian eruption. Stratigraphically this tephra layer is very important due to its close association with the marine isotope stage 3/2 transition or Heinrich Stadial 3 (HS3) (Negri et al., 1999). Subsequently this layer has been readily identified in numerous other Mediterranean archives and thus offers a crucial central Mediterranean regional marker layer (Fig. 1a) (Table 1; Munno and Petrosino, 2004, 2007; Wulf et al., 2004; Wagner et al., 2008; Zanchetta et al., 2008; Bourne et al., 2010; Caron et al., 2010; Vogel et al., 2010; Damaschke et al., 2013). The timing of this eruption and its widespread dispersal means that it offers significant potential to precisely synchronise archives, enabling the assessment of spatial leads and/or lags associated with an important environmental transition.

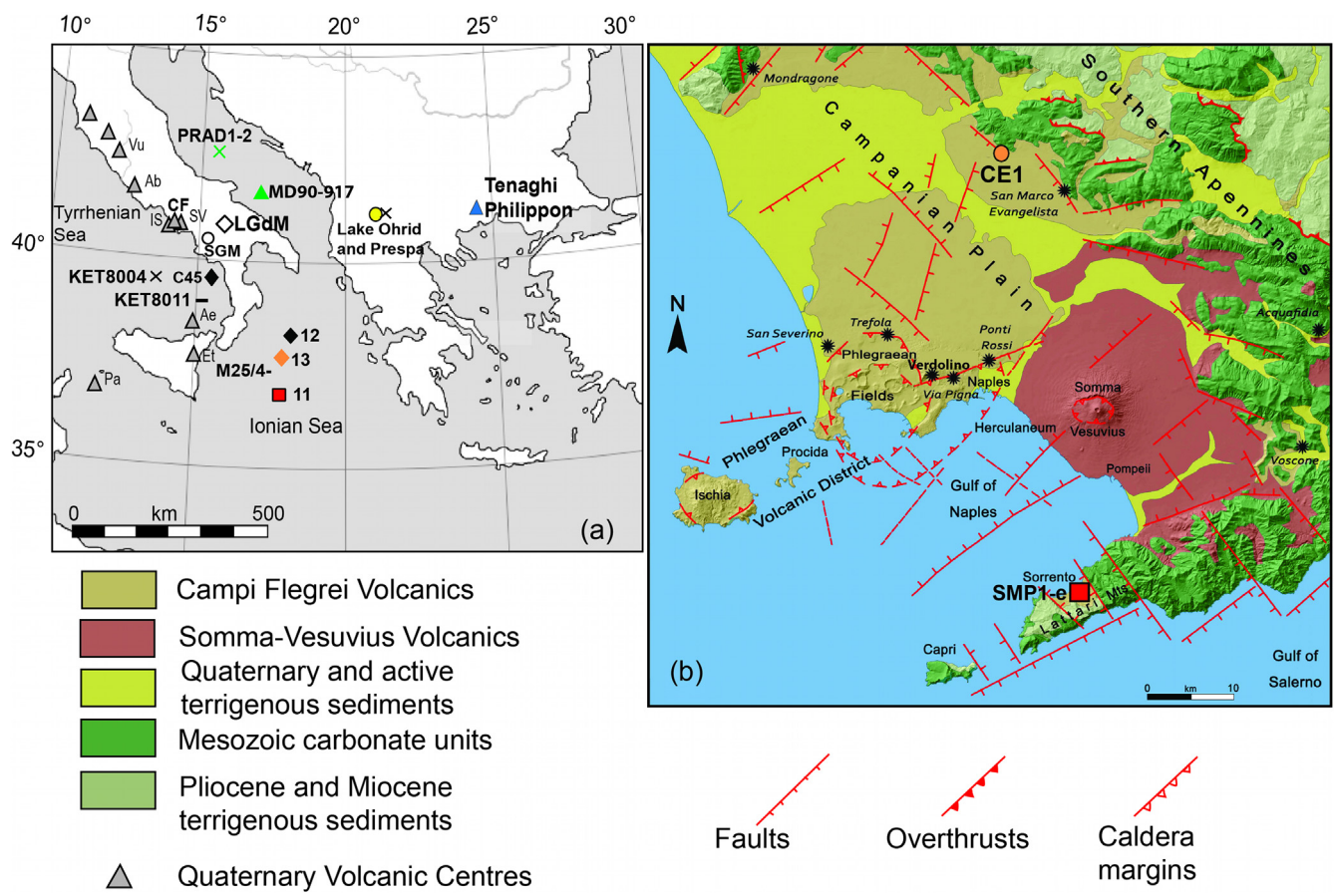


**Fig. 1.** (a) A map of the central and eastern Mediterranean showing the location of the M25/4-12 core from which the type locality Y-3 tephra was investigated. The localities of other archives where proposed 'Y-3' tephra correlatives have been reported (listed in Table 1). The main volcanic centres active during the Last Glacial (CF, Campi Flegrei; SV, Somma-Vesuvius; IS, Ischia, Ae, Aeolian Islands; Et, Mount Etna; Pa, Pantelleria) are marked. (b) The volcanoes in the Neapolitan volcanic region, Campi Flegrei, Somma-Vesuvius and Ischia (adapted from Tomlinson et al., 2012), and the localities of extra-caldera (SMP1-e and CE1) samples.

Please cite this article in press as: Albert, P.G., et al., Revisiting the Y-3 tephrostratigraphic marker: a new diagnostic glass geochemistry, age estimate, and details on its climatostratigraphical context, Quaternary Science Reviews (2014), http://dx.doi.org/10.1016/j.quascirev.2014.04.002

**Table 1**
Reported occurrence of the Y-3 tephra and proposed correlatives from across the Central Mediterranean region. Dispersal is given relative to Campi Flegrei caldera. Presented are ages associated with these tephra deposits. Terrestrial and marine radiocarbon ages are have been calibrated using atmospheric and marine data sets respectively incorporated within IntCal13. LGdM, Lago Grande di Monticchio and SGM, San Gregorio Magno basin. mp = micro-pumice. * Source and reference of age determination.

| Tephra/Archive | Depth (cm) | Thickness (cm) | Description | | Phenocrysts | Dispersal | Distance from CVZ (km) | Dating (method) | $^{14}$C (uncal) | Age cal. yrs BP | Reference |
|---|---|---|---|---|---|---|---|---|---|---|---|
| | | | Morphology | Colour | | | | | | | |
| *Y-3 'type locality' Ionian Sea* | | | | | | | | | | | |
| Y-3, Ionian Sea (RC 191) | 245–244 | 1 | – | Yellowish-grey layer | kf, ap, bt | SE | | – | – | – | Keller et al. (1978) |
| Y-3 (M25/4-12. M25/4-13*) | 117–118 | 1 | (1) HV tubular shards; (2) MV blocky shards | Yellowish-grey layer; clear to brown shards | kf, ap, bt | SE | 450 | $^{14}$C interpolation | – | *22,300 –28,300 | Kraml (1997)*; This Study |
| *Proximal 'Y-3' correlative* | | | | | | | | | | | |
| VRa (Verdolino Valley, CF) | – | 450 | HV pumice | Light beige (base) to brown (top) | plg, kf,cpx, bt, mag, minor ap | – | – | $^{40}$Ar/$^{39}$Ar | – | 30,300 ± 400 (2σ)*(29,900 –30,700) | Orsi et al. (1996); Pappalardo et al. (1999)*; Tomlinson et al. (2012) |
| *Medial 'Y-3' correlative* | | | | | | | | | | | |
| SMP1-e tephra | | | | | | | | | | | |
| SMP1-e, Sorrentine Peninsula (ZS 98262) | – | 40–50 | HV pumice | Light-grey | Aphyric, minor kf | SE | 30 | AMS $^{14}$C on charcoal from palaeosol directly beneath the tephra | 25,820 ± 270 | 29,390–30,720 | Sulpizio et al. (2003); Di Vito et al. (2008) |
| CE1, Cervino (ZS 2506 lower; ZS 2507 upper) | | 100 | HV pumice (lower) to MV pumice (upper) | Light-grey | Aphyric, minor kf | NE | 32 | – | – | – | |
| *Distal 'Y-3' correlatives* | | | | | | | | | | | |
| *Marine* | | | | | | | | | | | |
| Tyrrhenian Sea | | | | | | | | | | | |
| A2, Salerno Gulf core C-106 | 565–579 | 14 | – | – | kf, bt, cpx | S | | AMS $^{14}$C on foraminifera 4 cm below the tephra | 26,030 ± 150 | 29,350–30,310 | Buccheri et al. (2002a): Munno and Petrosino (2004) |
| B2, Salerno Gulf core C-45 | 380–383 | 3 | – | – | kf, bt, cpx | S | | AMS $^{14}$C on foraminifera 3 cm below the tephra | 25,570 ± 110 | 28,890–29,530 | Buccheri et al. (2002b); Munno and Petrosino (2004) |
| | | | | | | | | A2/B2 Integrated age (Bayesian age –depth model) | | 28,618–29,541 | Bronk Ramsey et al. (submitted for publication) |
| C-7, KET8004 | 264–274 | 10 | – | – | – | S | 100 | – | – | – | Paterne et al. (1988); Zanchetta et al. (2008) |
| C-7, KET8011 | 205 | 1 | – | – | – | S | 180 | – | – | – | Paterne et al. (1988); Zanchetta et al. (2008) |
| Adriatic Sea | | | | | | | | | | | |
| 920, MD90-917 | 920 | – | – | – | – | E | 260 | – | – | – | Zanchetta et al. (2008) |
| PRAD 1332, PRAD1-2 | 1332 | <1 | Vesicular shards | Clear | – | NE | 190 | AMS $^{14}$C on foraminifera 8 cm below the tephra | 24,130 ± 150 | 27,550–28,120 | Bourne et al. (2010); Piva et al. (2008) |
| | | | | | | | | AMS $^{14}$C on foraminifera 8 cm below the tephra | 23,390 ± 150 | 27,020–27,600 | Bourne et al. (2010); Piva et al. (2008) |

(*continued on next page*)

**Table 1** (*continued*)

| Tephra/Archive | Depth (cm) | Thickness (cm) | Description | | Phenocrysts | Dispersal | Distance from CVZ (km) | Dating (method) | $^{14}C$ (uncal) | Age cal. yrs BP | Reference |
|---|---|---|---|---|---|---|---|---|---|---|---|
| | | | Morphology | Colour | | | | | | | |
| Terrestrial (Italy/Balkans) | | | | | | | | | | | |
| TM-15, Lago Grande di Monticchio | 1471.9 | 28.6 | HV mp | Beige | kf, plg, bt, cpx | E | 120 | Varve Chronology | – | 27,260 ± 1360 | Wulf et al. (2004, 2012)*; Tomlinson et al. (2012) |
| S19, SGM basin | 665–700 | 35 | HV mp | – | Kf, bt | SE | 90 | – | – | – | Munno and Petrosino (2007) |
| 896 Oh, Lake Ohrid | 896–987 | 1 | HV tubular shards/mp | Yellowish-grey | Kf | E | 550 | | | | Wagner et al. (2008) |
| JO-188, Lake Ohrid | 185.5–188.5 | 3 | HV tubular shards/mp | Transparent to brown | – | E | 550 | – | – | – | Caron et al. (2010); Lezine et al. (2010) |
| OT0702-4, Lake Ohrid | 617–620 | 3 | (1) HV tubular; (2) Cuspate shards/mp | Light to brown | kf, plg, cpx | E | 550 | AMS bulk $^{14}C$ on sediment directly above the tephra layer | 25,260 ± 210 | 28,780–29,890 | Vogel et al. (2010) |
| PT0915-05, Lake Prespa | 616.8–617.8 | 1 | (1) HV tubular; (2) Cuspate shards/mp | Transparent to brown | – | E | 570 | – | | | Damaschke et al. (2013) |

However, complexity still surrounds the use of the Y-3 tephra as a precise stratigraphic and chronostratigraphic marker. The absence of detailed glass chemistry from the type locality Y-3 tephra means that existing distal correlations have not been subject to the necessary levels of geochemical validation. For this reason it is difficult to know which of the distal ages should be adopted for this marker tephra (Table 1). Determining the precise proximal counterpart of this tephra also presents a further uncertainty. Whilst it is generally regarded that the Y-3 tephra originates from an eruption within the Campi Flegrei (CF) caldera, southern Italy (Fig. 1) (Zanchetta et al., 2008), determining the proximal equivalent remains challenging due to more recent activity and limited exposure in this heavily developed region. Tephrostratigraphic investigations on deposits outside the caldera suggested that the SMP1-e (Santa Maria di Pozzano 1-e) ignimbrite deposits that are exposed along Sorrentine Peninsula (Fig. 1b) were the medial equivalent of the Y-3 tephra (Sulpizio et al., 2003; Di Vito et al., 2008). These deposits show similar stratigraphic, lithological, compositional, and chronological constraints to the distal marker (Table 1). Charcoal material from the palaeosol directly beneath the SMP1-e ignimbrite unit is dated to 29,390–30,720 cal yrs BP, which is older than the interpolated sapropel age of the Y-3 distal marine marker in the Ionian Sea (25.3 ± 3 ka; Kraml, 1997) (Table 1). These SMP1-e tephra deposits, in turn, are correlated to the 4.5 m thick intra-caldera surge and fall deposits of the VRa eruptive unit outcropping in the Verdolino Valley (VR) (Di Vito et al., 2008). The VRa unit represents a single eruption within the Tufi Biancastri stratigraphy (Orsi et al., 1996) – a series of CF eruptions that occurred between the two caldera forming eruptions, the Campanian Ignimbrite (CI)/Y-5 (39.28 ± 0.11 $^{40}Ar/^{39}Ar$ ka, De Vivo et al., 2001) and Neapolitan Yellow Tuff (NYT)/C-2 (14,320–13,900 cal yrs BP; Blockley et al., 2008a). Pappalardo et al. (1999) dated the VRa to 30.3 ± 0.2 ($1\sigma$) ka ($^{40}Ar/^{39}Ar$) which is consistent with the calibrated SMP1-e age (Table 1). Consequently, Zanchetta et al. (2008) suggested that the best age estimate for the Y-3 tephra was ca 30–31 cal ka BP.

Here we present the first shard-specific major, minor and trace element data for Y-3 glass shards from its type locality in the Ionian Sea (Keller et al., 1978; Kraml, 1997) to offer a definitive geochemical reference for this tephra. This data is used here to: (1) test proximal links to Campi Flegrei using glass data from the Tufi Biancastri units presented by Tomlinson et al. (2012); (2) assess links to medial-distal extra-caldera tephra deposits recorded on the Sorrentine Peninsula and within the Campanian Plain (i.e., SMP1-e tephra; Di Vito et al., 2008); and (3) use the diagnostic glass geochemistry of the type locality Y-3 to verify existing (see Table 1) and new distal–distal correlations that underpin the synchronisation of archives throughout the Mediterranean region. This will help verify the known dispersal of the Y-3 tephra and improve the chronological and environmental constraints placed upon this important tephrostratigraphic marker.

## 2. Materials

In this section we outline the tephra samples that have been subject to new detailed shard-specific major, minor and trace element geochemical analysis within this study.

### 2.1. Distal tephra samples

#### 2.1.1. Y-3 Ionian Sea (M25/4-12)

Reported here is the Y-3 tephra from the Ionian Sea core M25/4-12 (Fig. 1a), a 1 cm thick yellow–grey visible layer that occurs at 117.5–118.5 cm below the sea floor. Core M25/4-12 was retrieved with a piston corer from the Calabrian Rise 37°57′98″N;

18°11′04″E in the Central Ionian Sea at a 2473 m water depth on the *Meteor* cruise M25/4 in 1993 (Keller et al., 1996; Kraml, 1997). The tephra sits close to the MIS 2/3 transition in the oxygen isotope stratigraphy of the core (Negri et al., 1999). The glass shards are typically clear, with occasional brown shards, and these are all between 100 and 200 μm in size (major axis). Shards comprise of two main morphologies: (1) highly vesicular, tubular shards and; (2) less vesiculated, blocky/angular shards (Fig. 2a–f). Phenocrysts of sanidine, apatite and biotite are also observed within this tephra layer.

#### 2.1.2. TP 9.70 (TP-2005), Tenaghi Philippon, NE Greece

TP 9.70 is a cryptotephra layer reported and geochemically characterised here for the first time. It was identified within the TP-2005 core from the terrestrial site of Tenaghi Philippon (TP), NE Greece (Fig. 1a; see Pross et al., 2007, 2009, and Müller et al., 2011 for details on the site and core). This cryptotephra was detected and extracted following the procedures outlined in Blockley et al. (2005). Multiple peaks in cryptotephra concentrations were detected over a 60 cm interval, the largest peak in shard concentrations is found at the base of this interval (9.70 m) where concentrations were as high as 2060 shards/per gram of dry sediment. At 9.40 m and 9.10 m shard concentrations are lower, with 1030 and 56 shards per gram of dry sediment, respectively. For this reason, 9.70 m is defined as the depth of tephra deposition. Geochemical analysis of the glass shards throughout the 60 cm confirms that they are from the same eruption (Supplementary information) and this indicates the upwards reworking of tephra within the peat sequence (Hardiman, 2012). TP 9.70 glass shards were <80 μm (long axis) and comprised of two main morphologies; (1) highly vesicular, tubular shards and; (2) less vesiculated, more blocky and angular shards.

#### 2.1.3. PRAD 1332 (PRAD 1-2)

The PRAD 1332 cryptotephra was previously reported by Bourne et al. (2010) at a depth of 1332 cm in core PRAD 1-2 (Fig. 1a). Major element glass data was presented in Bourne et al. (2010) and here we present shard-specific trace element data. PRAD 1-2 was recovered from the western and upper flank of the Mid-Adriatic deep (42°40.34.7826′N; 14°46.13.5565′E) at a water depth of 185.5 m (Bourne et al., 2010). Further details relating to this tephra layer are presented in Table 1. The tephra layer resides stratigraphically just above the MIS 2/3 transition in the core's oxygen isotope stratigraphy (Piva et al., 2008).

### 2.2. Medial (extra-caldera) tephra samples

The SMP1-e extra-caldera tephra deposits outlined by Sulpizio et al. (2003) and Di Vito et al. (2008) are subject to new shard-specific major, minor and trace element characterisation in this study. Pumices from the SMP1-e type locality at Santa Maria di Pozzano (SMP), 30 km south-east of CF caldera along the Sorrentine Peninsula, are re-investigated (Fig. 1b). This deposit comprises of an ash unit with sparse light grey aphyric pumice lapilli (ZS 98262). These have been interpreted as pyroclastic density current deposits (Di Vito et al., 2008) (Table 1). The CE1 pumice deposits from Cervino, 32 km north-east of the CF caldera (Fig. 1b), are also re-analysed. These tephra comprise two, well sorted beds of light grey, aphyric pumice separated by an ash unit (lower ZS 2506; upper ZS 2507). Di Vito et al. (2008) suggest that these deposits were the fall component associated with the SMP1-e eruption.

## 3. Methods

The visible Ionian Sea Y-3 ash (M25/4-12) was washed, dried and handpicked under a light microscope. Both cryptotephra layers were identified and extracted following the procedures outlined in Blockley et al. (2005). Distal tephra shards and medial pumices were mounted in Struers Epofix epoxy resin. These resin stubs were sectioned, polished and carbon coated for analysis. Scanning electron and transmitted light microscopy was conducted to map the stubs and identify individual clasts to ensure the coupling of major and trace element analysis to a single grain.

### 3.1. Analytical methods

All new geochemical data was generated from analysis of individual juvenile clasts (volcanic glass shards or pumice). Major and minor element glass data was generated using a wavelength-dispersive JEOL 8600 electron micro-probe (EMP) at the Research Laboratory for Archaeology and the History of Art, University of Oxford. Operating conditions are the same as those used in Smith et al. (2011) and are presented along with secondary standards in the Supplementary information. The majority of the trace element glass data was generated using Laser Ablation Inductively Coupled Plasma Mass Spectrometry (LA-ICP-MS). Analyses were performed using an Agilent 7500es ICP-MS coupled to Resonetics 193 nm ArF excimer laser ablation in the Department of Earth Sciences, Royal Holloway, University of London. Operating conditions are the same as those in Tomlinson et al. (2010) and are presented along with secondary standards in the Supplementary information. Secondary standards analysed during both EMP and LA-ICP-MS runs were from the Max Plank institute (MPI-DING suite; Jochum et al., 2006). Shards that were too small to be analysed by LA-ICP-MS (<20 μm spots) were analysed using Secondary Ion Mass Spectrometry (SIMS) on a Cameca IMS 4f ion microprobe at the Istituto di Geoscienze e Georisorse (IGG), Pavia (Italy). The operating conditions used are the same as those in Schiano et al. (2001, 2004) and are presented along with the secondary standards in the supplementary information.

### 3.2. Bayesian age–depth modelling of TP-2005

The age–depth model for Tenaghi Philippon was constructed using Bayesian deposition modelling (e.g. Blockley et al., 2008b) and was undertaken in OxCal version 4.2 (Bronk Ramsey, 2001, 2009) using the internationally agreed IntCal13 calibration curve (Reimer et al., 2013).[1] The age model was developed using the '*P_Sequence*' function in OxCal with '*Boundary*' functions placed at changes in lithology in the TP-2005 stratigraphy (Müller et al., 2011). The final age model comprises 20 radiocarbon dates (Müller et al., 2011), and includes a newly modelled proximal age for the Cape Riva tephra (Santorini) of 21,890–22,420 yrs BP (Lee et al., 2013; remodelled using IntCal13) and an $^{40}Ar/^{39}Ar$ age for the Campanian Ignimbrite (39,280 ± 110 yrs BP, De Vivo et al., 2001). Both of these tephras form visible layers within the TP-2005 sequence labelled (TP 7.61 and TP 12.87 respectively; Müller et al., 2011). In order to find an optimal '*K value*' (a Poisson constraining parameter) the model was initially run using a low *K value* of 0.001 (as recommended by Bronk Ramsey, 2008 and Blockley et al., 2008a,b) and slowly increased until the '*Agreement Index*' ($A_{overall}$ and $A_{model}$) was no lower than 60% (Bronk Ramsey, 2008).

[1] Note all radiocarbon ages presented here (cal yrs BP) have been calibrated using the IntCal13 or Marine13 internationally accepted calibration curve (Reimer et al., 2013) at 2σ unless otherwise stated. Year 0 is 1950.

Please cite this article in press as: Albert, P.G., et al., Revisiting the Y-3 tephrostratigraphic marker: a new diagnostic glass geochemistry, age estimate, and details on its climatostratigraphical context, Quaternary Science Reviews (2014), http://dx.doi.org/10.1016/j.quascirev.2014.04.002

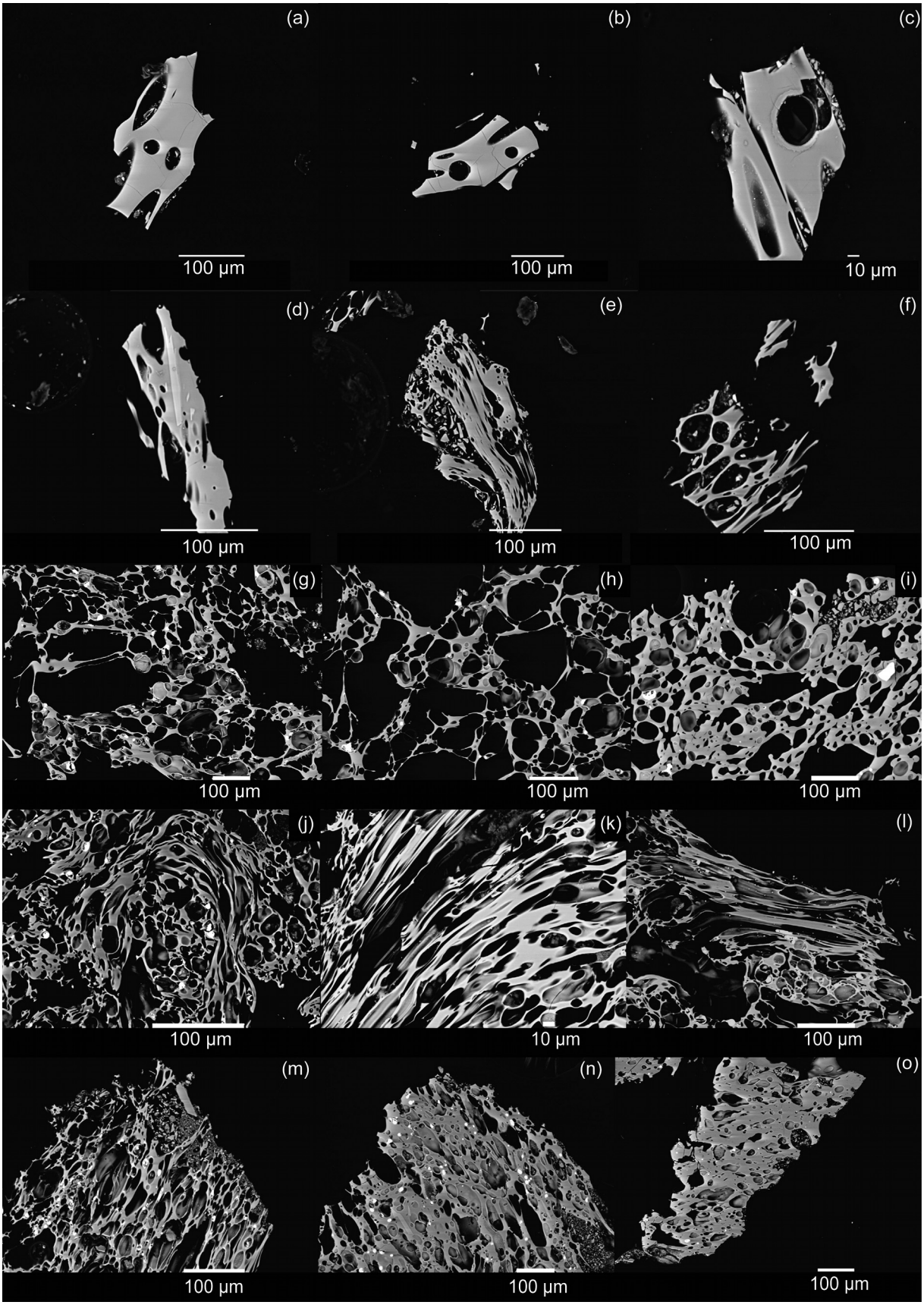


**Fig. 2.** SEM images of the distal and proximal tephras. Y-3 tephra recovered from M25/4-12 in the Ionian Sea (a–f); (a) shard 40D, a 20 μm ablation pit is observed left of a vesicle; (b) shard 29C, with two laser ablation pits (34 and 20 μm diameter); (c) shard 50E showing a 34 μm ablation pit; (d) shard 32D, a thin microlite is observed running through the glass shard, which demonstrates the benefit of preliminary SEM investigations prior to LA-ICP-MS analysis; (e) shard 51E; (f) shard 42D showing two ablation pits (34 and 20 μm); (g–h) the lower VRa, highly vesiculated white pumices (i) the upper VRa, less vesiculated, darker pumice; (j–l) SMP1-e (ZS 98262), highly vesicular and stretched pumices; (m) lower CE1 (ZS 2506) pumice, vesicular and stretched glasses; (n–m) upper CE1 (ZS 2507) pumices that are less vesiculated than the stratigraphically lower CE1 pumices.

Please cite this article in press as: Albert, P.G., et al., Revisiting the Y-3 tephrostratigraphic marker: a new diagnostic glass geochemistry, age estimate, and details on its climatostratigraphical context, Quaternary Science Reviews (2014), http://dx.doi.org/10.1016/j.quascirev.2014.04.002

No dates had to be removed from the model and the '*Date*' function was used to form realistic age estimates of undated horizons.

## 4. Results

Representative glass analyses from tephra units analysed in this study are given in Table 2. Full glass data sets for individual tephra deposits are presented in the Supplementary material. Table 3 presents diagnostic concentrations and ratios for the fingerprinting of individual tephra deposits. All these new results have also been integrated, where possible, with existing published glass data for proposed Y-3 tephra correlatives (Table 1).

### 4.1. Y-3 tephra, Ionian Sea – proximal source

The Ionian Sea Y-3 (M25/4-12) glasses are trachytic in composition, with some less evolved glasses falling close to the phonolite/trachyte boundary (Fig. 3a). The $K_2O$ (8.2–10.4 wt. %) contents are significantly higher than the $Na_2O$ (2.9–4.9 wt.%) contents, which is more consistent with a Campi Flegrei (CF) or Somma-Vesuvius source, rather than Ischia, where glasses show $Na_2O \geq K_2O$ (Fig. 4a–b). CaO concentrations at a given MgO clearly illustrates that the Ionian Sea Y-3 derives from Campi Flegrei and not Somma-Vesuvius (Fig. 4c). Major (i.e., 2.7–3.8 wt.% FeO and 2.0–2.8 wt.% CaO) and trace (i.e., 172–383 ppm Zr and 28–56 ppm Nb) element glass compositions of the Ionian Sea Y-3 tephra are heterogeneous (Fig. 5), with two distinct end-members and a few analyses plotting in-between (Fig. 5).

Two clear K-trachytic end-members are recognised within the Ionian Sea Y-3 glasses and are defined herein as; (1) the higher silica (>62 wt. % $SiO_2$) and; (2) the lower silica (<62 wt. % $SiO_2$) end-members. Zr/Sr ratios, reflective of magma evolution, clearly distinguish these two end-members (Table 3). The higher silica glasses show far greater levels of incompatible trace element enrichment (i.e., Th, Zr, Nb) than the lower silica glasses (Fig. 6; Table 2). Light Rare Earth Element (LREE) enrichment relative to the Heavy Rare Earth elements (HREE) differs between the two end-members (i.e., La/Yb), with the lower silica glasses displaying higher values (Table 3). Using increasing Th as a fractionation index V, Sr, Ba and Eu all show decreasing concentrations between the two end-members. The lower Sr, Ba and Eu concentrations in the higher silica glasses are likely to reflect greater K-feldspar (Sanidine) fractionation. Incompatible trace element ratios also differ between the two end-members (Table 3). Nb/Th ratios in the higher silica Y-3 glasses confirm the association of the tephra layer with the Tufi Biancastri/NYT series of CF deposits (Fig. 4d) (Tomlinson et al., 2012). Furthermore, vanadium concentrations in all the Y-3 glasses are consistently more elevated than observed in the Pre-CI/CI series glasses and again are consistent with the tephra being associated with the Tufi Biancastri/NYT series. The levels of incompatible trace element enrichment in the lower silica end-member glasses of the Y-3 tephra are lower than any currently characterised in the Tufi Biancastri/NYT series glasses (Fig. 4d) (Tomlinson et al., 2012).

The VRa eruptive unit is compositionally bimodal, like the Ionian Sea Y-3 tephra, with both a high and low silica trachyte end-member (Fig. 3). Both the major and trace element concentrations of the higher silica end-member of the VRa are the same as the high-silica trachytic glasses of the Ionian Sea Y-3 tephra (Figs. 3 and 6; Table 3). However, this high silica component of the Y-3 tephra is also compositionally similar to other stratigraphically younger Tufi Biancastri eruptive deposits (namely the VRb and PRa units; Figs. 3 and 5). Notwithstanding, the major element concentrations of the lower silica end-member of the Ionian Sea Y-3 tephra are significantly different to that of the VRa tephra (Fig. 3). The lower silica end-member of the Y-3 glasses have higher $SiO_2$, $K_2O$ and lower $TiO_2$, FeO, CaO, MgO and $Na_2O$ contents than the lower silica end-member of the VRa glasses (Fig. 3). Thus, the lower silica Y-3 glasses might appear intermediate in composition between the two end-members of the VRa glasses (Fig. 3). However, trace element variability between the two end-members of the VRa glasses is more restricted than that of the Ionian Sea Y-3 tephra (Fig. 5), thus inconsistent with their respective major element variability. Vanadium, Ba and Sr concentrations in the lower silica K-trachytic VRa glasses are higher than those in the lower silica Y-3 glasses. Plotting these elements against an incompatible element such as Th clearly illustrates that the Ionian Sea Y-3 tephra and the proximal VRa eruptive unit glasses lie on separate evolutionary trends (Fig. 6) and therefore are associated with different eruptions.

### 4.2. Y-3 Ionian Sea – medial correlatives

The SMP1-e ignimbrite deposits (ZS 98262) from the Sorrentine Peninsula have homogenous (i.e., 62.1 ± 0.5 wt.% $SiO_2$; 8.5 ± 0.2 wt.% $K_2O$) glass compositions and are classified as K-trachytes (Fig. 3a). The trace element compositions of the glasses are equally homogenous (i.e., 54 ± 3 ppm Nb; 29 ± 5 ppm Th; Fig. 5). The major and trace element compositions of these SMP1-e glasses are indistinguishable from the higher silica K-trachyte end-member of the Ionian Sea Y-3 tephra (Figs. 3, 5 and 6). Indeed, they share consistent incompatible trace element ratios and levels of LREE enrichment (Table 3).

The CE1 pumice fall beds from Cervino have glass compositions that are also homogeneous. The lower (ZS 2506) pumice fall glasses are fractionally more evolved (i.e., 58.1 ± 0.4 wt.% $SiO_2$) than the upper (ZS 2507) pumice fall glasses (57.7 ± 0.5 wt. % $SiO_2$). Both fall deposits classify as phonolites but lie close to the trachyte boundary (Fig. 3a). These phonolitic deposits have glass compositions that are clearly distinguishable from both end-members of the Ionian Sea Y-3 tephra and also the SMP1-e ignimbrite deposits. The CE1 glasses have major element compositions that partially overlap with the lower silica glasses of the proximal VRa eruptive unit (Fig. 3), but the trace element compositions of the lower (i.e., 27 ± 2 ppm Th) and the upper (i.e., 25 ± 2 ppm Th) CE1 glasses are clearly different from those of the VRa glasses (Fig. 6; Table 3). Most noticeable is that the CE1 glasses show more elevated Th concentrations than the lower silica VRa glasses (21 ± 2 ppm Th). The CE1 glasses also have incompatible trace element ratios that are offset from the currently available Tufi Biancastri/NYT series glasses (Tomlinson et al., 2012) (Fig. 6d; Table 3).

### 4.3. Y-3 Ionian Sea – distal correlatives

Glass shards from cryptotephra TP 9.70 recorded at TP have a heterogeneous major element composition (60.1–63.1 wt. % $SiO_2$; 8.1–10.0 wt. % $K_2O$) and show the same major element variability as the Ionian Sea Y-3 tephra (Figs. 3 and 5). Proposed Y-3 tephra correlatives (Table 1), MD90-917 920 (S. Adriatic; Zanchetta et al., 2008), OT0702-4/JO-188 (Lake Ohrid; Balkans; Vogel et al., 2010; Caron et al., 2010) and PT9015-05 (Lake Prespa, Balkans; Damaschke et al., 2013) all show major element variability that it is largely consistent with that of the Ionian Sea Y-3 and TP 9.70 Tenaghi Philippon (TP) layers (Figs. 3 and 5). These correlatives appear to comprise predominantly of intermediate glass compositions and extend towards either the higher or lower silica end-members of the Ionian Sea Y-3 tephra (Figs. 3 and 5). The TM-15 glasses from Lago Grande di Monticchio (LGdM; Wulf et al., 2004; Tomlinson et al., 2012), the S-19 tephra from San Gregorio Magno (SGM; Munno and Petrosino, 2004, 2007) basin, and the Tyrrhenian Sea ash layers (C-7, B2 and A2; Paterne et al., 1988; Buccheri et al.,

Please cite this article in press as: Albert, P.G., et al., Revisiting the Y-3 tephrostratigraphic marker: a new diagnostic glass geochemistry, age estimate, and details on its climatostratigraphical context, Quaternary Science Reviews (2014), http://dx.doi.org/10.1016/j.quascirev.2014.04.002

**Table 2**
Representative shard-specific major, minor (EMP) and trace element (LA-ICP-MS) glass data from the Ionian Sea Y-3 tephra (M25/4-12), extra-caldera CF deposits (SMP1-e and CE1), and other distal tephra deposits considered as potential correlatives of the Y-3 tephra including TP 9.70 (Tenaghi Philippon, NE Greece) and PRAD 1332 (PRAD 1-2, Central Adriatic). (LA, LA-ICP-MS analyses). A full grain-specific glass data set is presented in the Supplementary information. * Water-free major element data for PRAD1332 (Bourne et al., 2010) was calculating assuming a 0.4 wt.% Cl prior to normalisation.

| Sample | Y-3 Ionian Sea | | | | Extra-caldera, Tufi Binacastri | | | | | | TP 9.70 Tenaghi Philippon, Greece | | | | PRAD 1332 Central Adriatic | | | |
|---|---|---|---|---|---|---|---|---|---|---|---|---|---|---|---|---|---|---|
| Core/locality | (M25/4-12) | | | | SMP1-e (ZS 98286) | | CE1 Lower (ZS 2506) | | CE1 Upper (ZS 2507) | | TP-2005 | | | | PRAD 1-2 | | | |
| I.D | 31C | 29C | 18B | 28C | 9 | 2 | 23 | 8 | 1 | 13 | 384_22 | 384_21 | 334_5 | 332_14 | 0068_107 | 0068_8 | 0068_6 | 0068_113 |
| *Major, minor* | | | | | | | | | | | | | | | Bourne et al. (2010)* | | | |
| $SiO_2$ | 60.53 | 60.92 | 62.23 | 62.75 | 62.51 | 62.03 | 57.93 | 58.35 | 58.23 | 57.44 | 60.54 | 61.59 | 62.73 | 62.83 | 58.07 | 57.77 | 61.19 | 61.28 |
| $TiO_2$ | 0.40 | 0.36 | 0.34 | 0.34 | 0.36 | 0.41 | 0.53 | 0.51 | 0.54 | 0.59 | 0.35 | 0.31 | 0.36 | 0.38 | 0.64 | 0.61 | 0.45 | 0.43 |
| $Al_2O_3$ | 18.35 | 18.43 | 17.82 | 17.81 | 17.79 | 17.90 | 19.16 | 18.60 | 18.78 | 18.66 | 18.71 | 18.29 | 18.16 | 18.36 | 18.26 | 18.52 | 18.30 | 18.13 |
| FeOt | 3.77 | 3.27 | 2.77 | 2.82 | 2.79 | 3.01 | 4.53 | 4.65 | 4.37 | 4.88 | 3.63 | 3.19 | 2.78 | 2.94 | 5.20 | 5.16 | 3.68 | 3.63 |
| MnO | 0.11 | 0.12 | 0.10 | 0.08 | 0.12 | 0.14 | 0.15 | 0.11 | 0.15 | 0.21 | 0.10 | 0.09 | 0.09 | 0.12 | 0.15 | 0.12 | 0.10 | 0.11 |
| MgO | 0.83 | 0.74 | 0.35 | 0.45 | 0.43 | 0.40 | 1.16 | 1.06 | 1.26 | 1.36 | 0.81 | 0.55 | 0.49 | 0.42 | 1.51 | 1.53 | 0.75 | 0.75 |
| CaO | 2.63 | 2.60 | 2.28 | 2.10 | 2.03 | 2.22 | 3.70 | 3.67 | 3.98 | 4.27 | 2.71 | 2.30 | 2.33 | 2.14 | 4.12 | 4.25 | 2.91 | 2.90 |
| $Na_2O$ | 2.98 | 3.27 | 4.50 | 4.33 | 4.57 | 4.76 | 3.67 | 3.72 | 3.43 | 3.58 | 2.66 | 3.67 | 3.87 | 4.16 | 3.47 | 3.54 | 3.86 | 3.55 |
| $K_2O$ | 9.96 | 9.76 | 8.75 | 8.51 | 8.61 | 8.32 | 8.38 | 8.47 | 8.42 | 8.22 | 9.96 | 9.31 | 9.08 | 8.59 | 8.15 | 8.09 | 8.34 | 8.81 |
| $P_2O_5$ | 0.14 | 0.14 | 0.05 | 0.09 | 0.10 | 0.09 | 0.28 | 0.34 | 0.30 | 0.30 | 0.18 | 0.13 | 0.10 | 0.06 | *0.41* | *0.41* | *0.42* | *0.42* |
| Cl | 0.30 | 0.38 | 0.81 | 0.71 | 0.71 | 0.72 | 0.52 | 0.52 | 0.55 | 0.50 | 0.34 | 0.55 | – | – | – | – | – | – |
| Analytical total | 95.26 | 97.79 | 98.59 | 94.91 | 95.87 | 94.06 | 93.93 | 95.11 | 99.02 | 98.32 | 98.47 | 97.58 | 97.15 | 94.99 | 97.69 | 98.29 | 95.99 | 96.01 |
| *Trace* | | | | | | | | | | | | | | | | | | |
| Spot size | 34 μm | 34 μm | 34 μm | 20 μm | 34 μm | 34 μm | 34 μm | 34 μm | 34 μm | 34 μm | 5 μm | 5 μm | 34 μm | 5 μm | 25 μm | 25 μm | 25 μm | 25 μm |
| Method | LA | LA | LA | LA | LA | LA | LA | LA | LA | LA | SIMS | SIMS | LA | SIMS | LA | LA | LA | LA |
| V | 68.9 | 56.3 | 29.8 | 31.1 | 31.7 | 30.4 | 106.0 | 110.9 | 121.3 | 127.3 | 77.0 | 40.1 | 41.9 | 38.2 | 128.4 | 136.1 | 90.1 | 75.7 |
| Rb | 268 | 276 | 344 | 355 | 356 | 324 | 326 | 309 | 317 | 314 | 216 | 272 | 347 | 334 | 330 | 310 | 321 | 337 |
| Sr | 597 | 508 | 138 | 134 | 128 | 123 | 697 | 701 | 799 | 795 | 599 | 415 | 341 | 168 | 742 | 723 | 639 | 609 |
| Y | 19.2 | 22.0 | 31.5 | 29.8 | 29.7 | 29.9 | 25.8 | 26.4 | 26.4 | 25.0 | 17.5 | 23.6 | 27.9 | 27.1 | 24.6 | 24.1 | 23.8 | 24.1 |
| Zr | 172 | 223 | 370 | 370 | 358 | 354 | 277 | 273 | 281 | 264 | 168 | 250 | 307 | 348 | 257 | 237 | 256 | 267 |
| Nb | 30 | 38 | 53 | 55 | 56 | 53 | 45 | 44 | 43 | 41 | 22 | 38 | 48 | 51 | 40 | 37 | 40 | 41 |
| Ba | 801 | 636 | 24 | 32 | 26 | 26 | 1176 | 1194 | 1354 | 1376 | 880 | 315 | 182 | 47 | 1296 | 1257 | 1064 | 1051 |
| La | 43 | 48 | 71 | 67 | 65 | 66 | 69 | 66 | 65 | 63 | 41 | 45 | 63 | 56 | 50 | 48 | 50 | 51 |
| Ce | 79 | 96 | 134 | 131 | 129 | 128 | 130 | 129 | 132 | 126 | 78 | 89 | 116 | 122 | 97 | 94 | 99 | 97 |
| Pr | 8.4 | 10.0 | 13.9 | 13.3 | 13.2 | 12.7 | 13.6 | 13.4 | 13.6 | 12.9 | – | – | 12.8 | – | 11.0 | 9.9 | 10.2 | 10.4 |
| Nd | 31.1 | 37.2 | 49.3 | 48.8 | 47.7 | 48.6 | 51.9 | 48.4 | 50.2 | 47.8 | 25.9 | 31.5 | 43.9 | 48.8 | 40.3 | 39.5 | 39.4 | 38.5 |
| Sm | 6.1 | 6.3 | 8.3 | 10.1 | 8.3 | 9.2 | 9.2 | 9.3 | 9.5 | 9.1 | 4.3 | 4.7 | 8.3 | 8.4 | 7.8 | 7.9 | 6.8 | 6.4 |
| Eu | 1.9 | 1.8 | 1.6 | 1.5 | 1.6 | 1.6 | 2.2 | 2.1 | 2.2 | 2.1 | 1.3 | 1.4 | 1.9 | 1.7 | 2.0 | 1.9 | 1.9 | 1.7 |
| Gd | 4.5 | 5.0 | 6.0 | 8.1 | 6.3 | 6.5 | 6.7 | 6.5 | 6.6 | 6.7 | 3.7 | 3.8 | 7.2 | 6.5 | 5.5 | 5.9 | 5.7 | 5.5 |
| Dy | 3.6 | 4.9 | 5.6 | 5.7 | 5.0 | 5.3 | 5.3 | 5.2 | 5.1 | 4.9 | 3.5 | 3.8 | 5.3 | 5.3 | 4.9 | 4.6 | 4.7 | 4.3 |
| Er | 1.8 | 2.3 | 3.1 | 3.1 | 2.9 | 3.1 | 2.7 | 2.7 | 2.6 | 2.4 | 2.0 | 2.2 | 2.7 | 2.9 | 2.4 | 2.5 | 2.4 | 2.3 |
| Yb | 1.7 | 2.3 | 3.3 | 2.9 | 2.9 | 3.0 | 2.5 | 2.7 | 2.3 | 2.3 | 1.8 | 1.7 | 2.8 | 2.7 | 2.3 | 2.5 | 2.4 | 2.2 |
| Lu | 0.27 | 0.28 | 0.45 | 0.49 | 0.39 | 0.39 | 0.43 | 0.40 | 0.38 | 0.36 | – | – | 0.32 | – | 0.34 | 0.38 | 0.34 | 0.32 |
| Ta | 1.5 | 1.9 | 2.7 | 2.8 | 2.7 | 2.4 | 2.4 | 2.2 | 2.1 | 2.1 | – | – | 2.2 | – | 1.8 | 1.9 | 2.0 | 2.0 |
| Th | 13.2 | 16.7 | 30.7 | 29.9 | 28.7 | 28.6 | 27.3 | 26.3 | 25.9 | 24.7 | 12.1 | 22.3 | 25.7 | 30.5 | 21.2 | 20.1 | 23.6 | 23.1 |
| U | 4.4 | 5.8 | 9.9 | 10.1 | 9.6 | 8.8 | 9.1 | 8.6 | 7.9 | 7.9 | 3.5 | 6.3 | 8.9 | 8.9 | 7.3 | 7.2 | 8.0 | 8.0 |

**Table 3**
Diagnostic concentrations and ratios for geochemical fingerprinting the Y-3 tephra, errors are 2 standard deviations. TAS classification is based on ($Na_2O + K_2O$) versus $SiO_2$ using Le Bas et al. (1986). TP 9.70 data are representative analysis from each compositional end-member.

| Sample | M25/4-12_118.5- Y3 | | VRb | VRa | | C.I. (Fall) | C.I (Main flows) | C.I. Upper flow |
|---|---|---|---|---|---|---|---|---|
| Locality | Ionian Sea (This study) | | Verdoline Valley | Verdoline Valley | | Voscone & Aquafidia | Mondragone | Mondragone |
| TAS classification | Low $SiO_2$ Trachyte | High $SiO_2$ Trachyte | Trachyte | Low $SiO_2$ Trachyte | High $SiO_2$ Trachyte | Phonolite to Trachyte | Phonolite to Trachyte | Trachyte |
| | (This study) | | Tomlinson et al. (2012) | | | | | |
| FeO/CaO | 1.3 ± 0.1 | 1.3 ± 0.1 | 1.2 ± 1 | 1.3 ± 0.1 | 1.3 ± 1 | 1.6 ± 0.2 | 1.8 ± 0.1 | 1.3–2.2 |
| Cl wt. % | 0.36 ± 0.06 | 0.72 ± 0.11 | 0.45 ± 0.06 | 0.42 ± 0.05 | 0.49 ± 0.11 | 0.63 ± 0.06 | 0.85 ± 0.07 | 0.24–0.62 |
| V (ppm) | 63 ± 10 | 31 ± 1 | 51 ± 8 | 121 ± 14 | 38 ± 5 | 16 ± 4 | 14 ± 2 | 15–64 |
| Zr/Sr | 0.34 ± 0.11 | 2.69 ± 0.15 | 0.92–2.42 | 0.35 ± 0.02 | 0.94–2.58 | 5–31 | 8–28 | 0–39 |
| Nb/Th | 2.1 ± 0.2 | 1.8 ± 0.1 | 1.9 ± 0.3 | 1.9 ± 0.1 | 1.9 ± 0.1 | 2.4 ± 0.1 | 2.4 ± 0.2 | 2.1–2.5 |
| Zr/Th | 13.1 ± 0.6 | 11.9 ± 0.5 | 11.2 ± 1.1 | 12.0 ± 0.4 | 12.2 ± 0.3 | 13.4 ± 0.6 | 12.7 ± 0.6 | 11.8–13.4 |
| Ta/Th | 0.10 ± 0.02 | 0.09 ± 0.01 | 0.09 ± 0.01 | 0.09 ± 0.003 | 0.09 ± 0.01 | 0.11 ± 0.004 | 0.11 ± 0.01 | 0.16–0.19 |
| Nb/Zr | 0.16 ± 0.02 | 0.15 ± 0.01 | 0.17 ± 0.01 | 0.16 ± 0.004 | 0.15 ± 0.01 | 0.18 ± 0.01 | 0.19 ± 0.01 | 0.10–1.13 |
| Y/Th | 1.41 ± 0.12 | 1.00 ± 0.03 | 1.01 ± 0.1 | 1.15 ± 0.04 | 1.06 ± 0.1 | 1.04 ± 0.1 | 1.06 ± 0.06 | 1.0–1.5 |
| La/Yb | 24.5 ± 3.6 | 22.7 ± 2.7 | 25.5 ± 1.4 | 22 ± 1.7 | 23.1 ± 1.5 | 22.8 ± 1.7 | 23.2 ± 2.1 | 23.6 ± 2.1 |

| Sample | SMP1-e | | | TM-15 | PRAD 1332 | | TP-9.70 | |
|---|---|---|---|---|---|---|---|---|
| Locality | SMP1-e | CE1 | | LGdM | PRAD1-2 | | Tenaghi Philippon | |
| TAS classification | Trachyte | Phonolite | | Trachyte | Low $SiO_2$ Trachyte | High $SiO_2$ Trachyte | Low $SiO_2$ Trachyte | High $SiO_2$ Trachyte |
| | (ZS 98262; This study) | (ZS 2506; This study) | (ZS 2507; This study) | Tomlinson et al. (2012) | (This study) | | (This study) | |
| FeO/CaO | 1.4 ± 0.1 | 1.2 ± 0.1 | 1.2 ± 0.1 | 1.3 ± 0.1 | 1.2 ± 0.1 | 1.2 ± 0.1 | 1.3 | 1.3 |
| Cl wt. % | 0.71 ± 0.08 | 0.54 ± 0.06 | 0.50 ± 0.05 | 0.57 ± 0.21 | – | – | 0.45 | 0.54 ± 0.24 |
| V (ppm) | 31 ± 3 | 107 ± 7 | 122 ± 10 | 40 ± 10 | 128 ± 16 | 87 ± 20 | 77 | 38.2 |
| Zr/Sr | 2.82 ± 0.41 | 0.40 ± 0.03 | 0.34 ± 0.03 | 0.52–2.65 | 0.34 ± 0.03 | 0.42 ± 0.04 | 0.28 | 2.07 |
| Nb/Th | 1.8 ± 0.2 | 1.7 ± 0.1 | 1.7 ± 0.2 | 1.8 ± 0.1 | 1.9 ± 0.1 | 1.8 ± 0.1 | 2.3 | 1.7 |
| Zr/Th | 12 ± 1.0 | 10.4 ± 0.7 | 10.9 ± 1.3 | 12.2 ± 0.5 | 11.8 ± 0.7 | 11.6 ± 1.0 | 14.2 | 11.4 |
| Ta/Th | 0.09 ± 0.01 | 0.08 ± 0.01 | 0.08 ± 0.02 | 0.09 ± 0.01 | 0.09 ± 0.01 | 0.09 ± 0.01 | – | – |
| Nb/Zr | 0.15 ± 0.01 | 0.16 ± 0.01 | 0.16 ± 0.01 | 0.15 ± 0.01 | 0.16 ± 0.01 | 0.15 ± 0.01 | 0.13 | 0.15 |
| Y/Th | 1.00 ± 0.09 | 0.99 ± 0.08 | 1.03 ± 0.08 | 1.09 ± 0.1 | 1.17 ± 0.07 | 1.04 ± 0.09 | 1.45 | 0.89 |
| La/Yb | 22.5 ± 2.4 | 27.1 ± 3.4 | 25.5 ± 2.7 | 23.2 ± 2.9 | 21.0 ± 2.9 | 21.3 ± 2.9 | 22.2 | 20.6 |

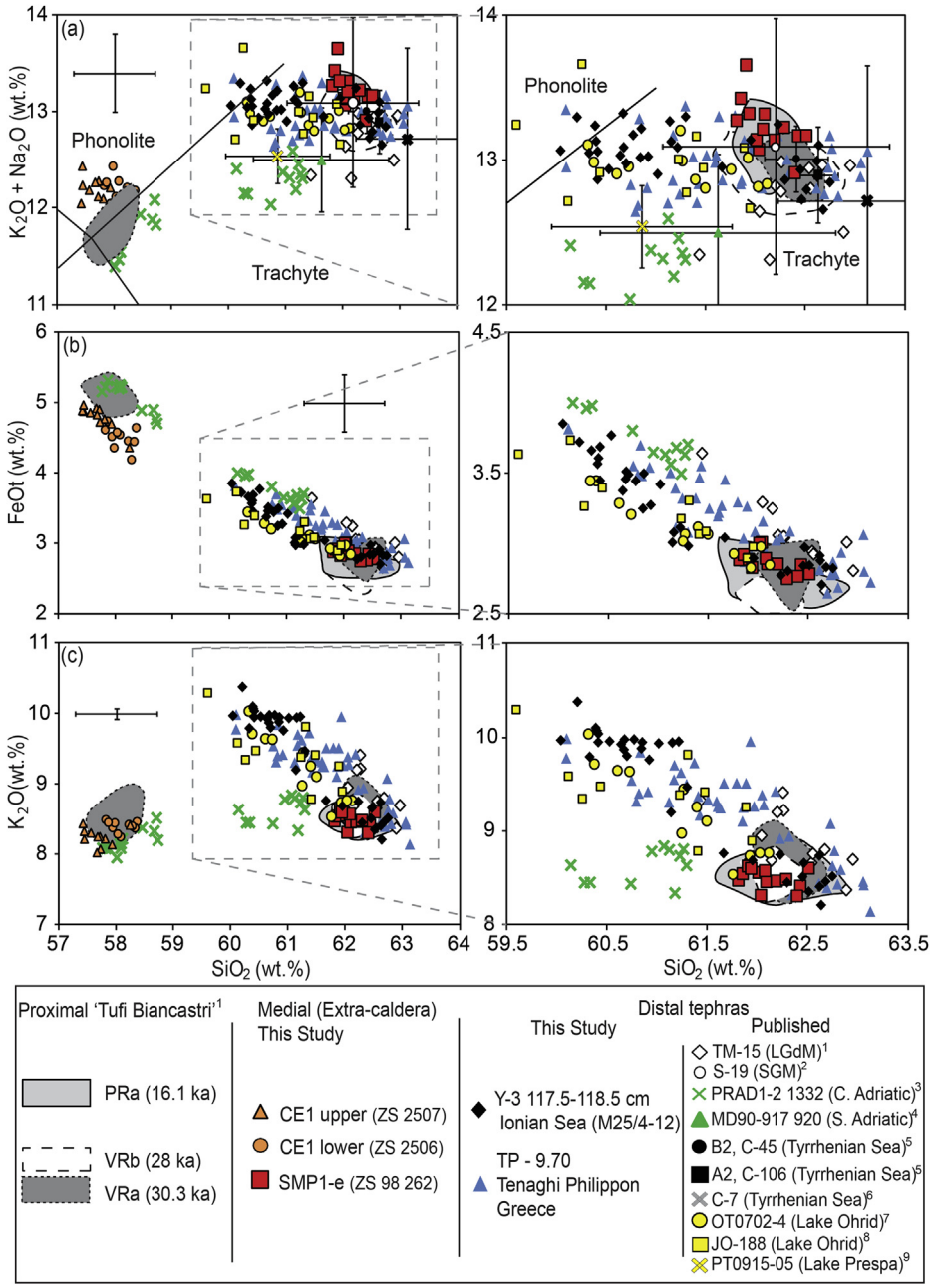


**Fig. 3.** Major element bi-plots showing the glass compositions of Ionian Sea Y-3 tephra (M25/4-12) compared to those of proximal intra-caldera Tufi Biancastri (Tomlinson et al., 2012) and extra-caldera deposits (SMP1-e, CE1; this Study) from Campi Flegrei. Glass data from cryptotephra TP 9.70 layer in Tenaghi Philippon, NE Greece (This study). Published glass compositions of distal layers (Table 1) are also presented to assess distal–distal tephra correlations: References are as follows; (1) Tomlinson et al. (2012); (2) Munno and Petrosino, 2007; (3) Bourne et al. (2010)*; (4) Zanchetta et al. (2008); (5) Munno and Petrosino (2004); (6) Paterne et al. (1988), Zanchetta et al. (2008); (7) Vogel et al. (2010); Caron et al. (2010); (9) Damaschke et al. (2013). Error bars represent 2 standard deviations of repeat analyses of the StHs6/80-G MPI-DING reference glass. (a) TAS classification after Le Bas et al. (1986). *Water-free major element data for PRAD1332 (Bourne et al., 2010) was calculating assuming a 0.4 wt.% Cl prior to normalisation.

2002a, 2002b; Munno and Petrosino, 2004) (Table 1) all appear to be restricted to the higher silica trachytic end-member of the Ionian Sea Y-3 tephra (Fig. 3a).

The trace element glass compositions of cryptotephra TP 9.70 are heterogeneous (168–420 ppm Zr; 28–56 ppm Nb) with a compositional range consistent with those of the Ionian Sea Y-3 tephra (Figs. 5 and 6). The TP 9.70 glasses present compositions that are consistent with both end-members of the Ionian Sea Y-3 and this is reflected in their comparable incompatible trace element ratios (Table 3). Crucially, the TP 9.70 glasses lie upon the same evolution trends as the Ionian Sea Y-3 tephra, best demonstrated by V, Sr and Ba concentrations relative to Th (Fig. 6a–c). TP 9.70 glasses are dominated by trace element compositions that are intermediate between to the two end-members of the Ionian Sea Y-3 tephra. TM-15 (LGdM) glasses do not display as much trace element heterogeneity as either the Ionian Sea Y-3 tephra or cryptotephra TP 9.70 and this is consistent with the absence of a lower silica K-trachytic end-member at a major element level (Fig. 3). However using V, Sr and Ba plotted against Th it is clear that the TM-15 glasses fall upon the same diagnostic trends as the Ionian Sea Y-3 tephra, which is different from the VRa eruptive unit (Fig. 6). The presence of intermediate compositions also demonstrates particularly good geochemical agreement with the cryptotephra TP 9.70 (Fig. 6).

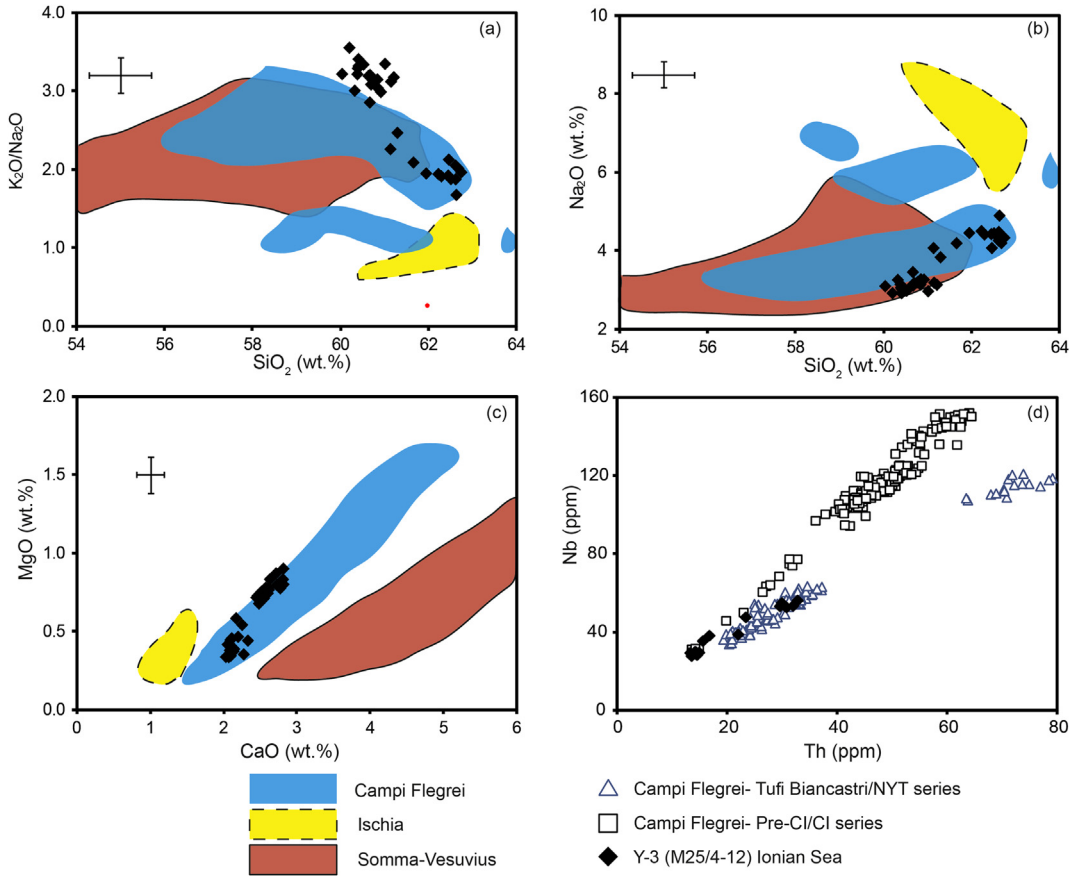


**Fig. 4.** Major and trace element glass compositions of the Ionian Sea Y-3 tephra (M25/4-12) compared to proximal Campi Flegrei (Tomlinson et al., 2012), Somma-Vesuvius (Tomlinson et al. unpublished[1]) and Ischia (Tomlinson et al., submitted for publication) tephra deposits. (a–c) Y-3 glasses compared to the glass compositional fields of the Neapolitan volcanic centres; and (d) Y-3 glass compositions plotted against those of the pre- and post-Campanian Ignimbrite series (Tomlinson et al., 2012). Error bars represent 2 standard deviations of repeat analyses of the StHs6/80-G reference glass. [1]Vesuvius glass data used to evaluate potential geochemical links and to generate this compositional field is available on the RESET database (https://c14.arch.ox.ac.uk/login/login.php?Location=/resetdb/db.php).

The major element glass compositions of the bimodal central Adriatic tephra layer PRAD 1332 do not correspond with either end-member of the Ionian Sea Y-3 tephra (Fig. 3). The higher silica K-trachyte component of the PRAD 1332 glasses have noticeably lower $K_2O$ and slightly higher CaO than the Ionian Sea Y-3 tephra glasses at a similar silica concentration (Figs. 3c, 5b). The lower silica trachyte component of the PRAD 1332 layer instead corresponds to the lower silica trachytic end-member of the VRa eruptive unit (Fig. 3). At a trace element level the bi-modality of the PRAD 1332 tephra is best observed by the clear differences in Ba, Sr and V concentrations (Table 3), the lower silica component shows higher concentrations of these elements compared to the higher silica component (Fig. 6) and is consequently less evolved (lower Zr/Sr ratio; Table 3). As with their major element compositions, the trace element concentrations and incompatible element ratios of the lower silica K-trachyte glasses in the PRAD 1332 layer are similar to the compositional field of the lower silica VRa glasses (Fig. 6; Table 3). The higher silica PRAD 1332 glasses fall on the evolutionary trend between the two end-members of the VRa glasses (Fig. 6).

## 5. Discussion

### 5.1. Y-3 tephra correlations

The new glass data presented here for the type locality Ionian Sea Y-3 tephra confirms that the tephra is associated with a Campi Flegrei (CF) eruption and is consistent with an event from the Tufi Biancastri/NYT series (cf. Tomlinson et al., 2012) (Fig. 4d). This information coupled with its stratigraphic position (above the Y-5/Campanian Ignimbrite) and chronological constraints (25.3 ± 3 ka; Table 1) are evidence for the Ionian Sea Y-3 tephra being erupted between the caldera forming CI and NYT eruptions (an eruption in the Tufi Biancastri sequence). The high silica K-trachyte end-member of the Ionian Sea Y-3 clearly verifies this affinity to the Tufi Biancastri Series glasses (Figs. 3 and 6). Unfortunately, a high silica (61.5–62.5 wt. %), K-trachyte glass chemistry is repeatedly erupted through time as it is recorded in successive units within the Tufi Biancastri stratigraphy (i.e., VRa, VRb and PRa; Fig. 3). Consequently, this means that this geochemical component alone is not diagnostic (Tomlinson et al., 2012) or useful for precisely establishing the proximal equivalent of this distal tephra. The eruption of repeat major element glass compositions at CF is not unique to the Tufi Biancastri deposits, many Holocene eruptive deposits are also compositionally indistinguishable (i.e., Smith et al., 2011).

It is the presence of the full compositional variability and in particular the identification of the lower silica (ca 60–61.5 wt.%) end-member of the Ionian Sea Y-3 tephra that is diagnostic of this marker layer (Fig. 3, 5 and 6). However, trace element concentrations confirm that the Ionian Sea Y-3 and the VRa are not from the same eruption, as the two tephra lie upon separate evolutionary trends (Fig. 6). Consequently, the $^{40}Ar/^{39}Ar$ of the VRa should not be exported distally to the Y-3 tephra.

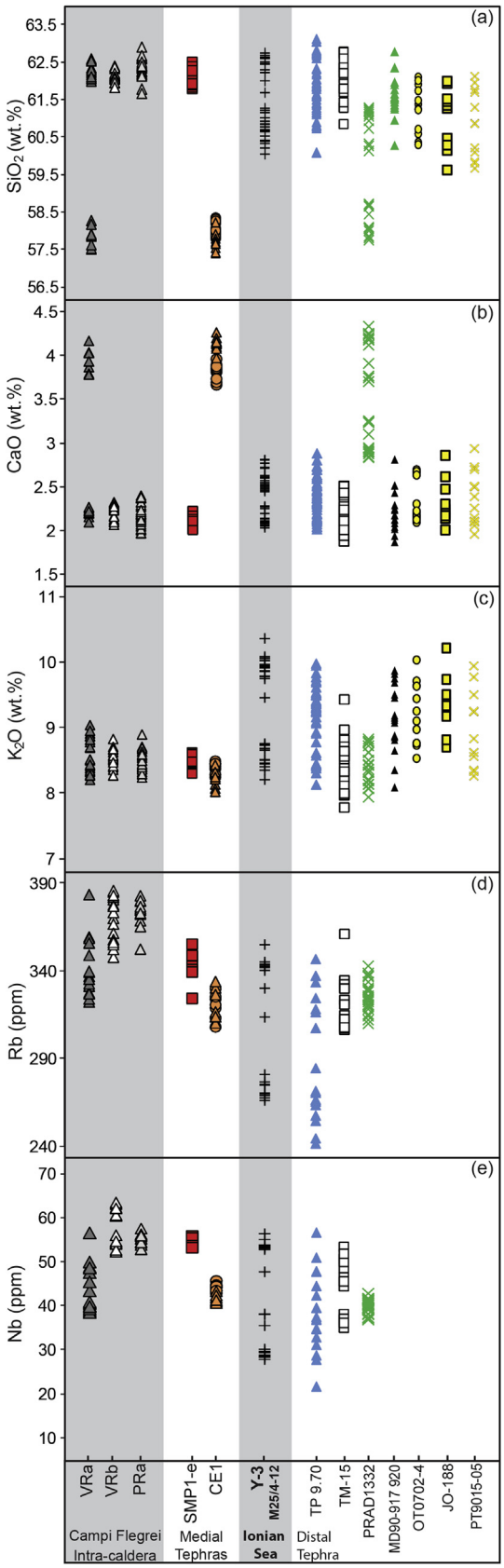


**Fig. 5.** Major and trace element compositional variation of glasses from the Y-3 tephra recorded in the Ionian Sea compared to potential proximal, medial and distal tephra correlatives. The Ionian Sea Y-3 glasses are dominated by two compositional end-members, whilst the Tenaghi Philippon tephra spans the full compositional range. Refer to Fig. 3 figure caption for published data references.

The absence of a precise proximal equivalent of the Ionian Sea Y-3 tephra illustrates a need for further grain-specific geochemical characterisation of more proximal Tufi Biancastri eruptive units. However, the potential for identifying the proximal equivalent of the distal tephra at CF is likely to be restricted by the complexity of the proximal volcanic stratigraphy, where often only limited exposure is available, particularly given that subsequent caldera collapse (NYT) has destroyed and/or buried many of the older pyroclastic units (Di Vito et al., 2008). The absence of a proximal age places further emphasis on establishing precise medial and distal tephra correlations in order to resolve the age of this distal marker.

At extra-caldera localities, the SMP1-e ignimbritic tephra recorded on the Sorrentine Peninsula (Fig.1b) does not present the full diagnostic compositional heterogeneity of the Ionian Sea Y-3 tephra (Fig. 3–5). Only the high silica trachytic end-member of the Ionian Sea Y-3 is identified and, given that this composition is repeatedly erupted in this timeframe, a correlation with the Ionian Sea Y-3 marker remains inconclusive based on glass chemistry alone. The proposed fall component of the SMP1-e eruption, the CE1 tephra deposits, NE of Campi Flegrei (Fig. 1b), are not medial a equivalent of the Y-3 tephra or the VRa eruptive unit (Fig. 6). Furthermore, the new glass data raises doubt over the stratigraphic correlation of both the SMP1-e (ignimbritic) and CE1 (fall) units under a single SMP1-e eruptive deposit (Di Vito et al., 2008). These units have different incompatible trace element ratios (Table 3) and this, combined with the absence of intermediate compositions between their respective compositions, means that it is difficult to envisage them as being related to the same CF eruption (Fig. 5). Consequently, the CE1 tephra fall deposits should no longer be chronologically constrained by the age of the SMP1-e ignimbrite deposits (Table 1). This interpretation emphasises the frequency of explosive activity at CF, and the difficulty of stratigraphically correlating proximal and medial tephra deposits based only on limited exposure.

Currently, neither the extra- or intra-caldera deposits analysed fully satisfy the diagnostic compositional variability of the Ionian Sea Y-3 tephra (Figs. 3, 5 and 6). The high silica K-trachytic end-member is characteristic of most post CI/pre-NYT CF eruptions and thus this component is not diagnostic. Fortunately, the compositional range of the Ionian Sea Y-3 tephra, in particular the presence of the lower silica trachytic end-member, is diagnostic of this marker layer. Consequently, it is important to use the full diagnostic geochemical signature of the Ionian Sea Y-3 tephra when attempting to validate Y-3 tephra correlations.

The Ionian Sea Y-3 glass data unequivocally confirms an eastern ash dispersal associated with this CF eruption (Fig. 3, 5 and 6). The cryptotephra TP 9.70 recorded at TP, NE Greece, corresponds precisely to the Ionian Sea Y-3 tephra (Fig. 3, 5 and 6). This correlation extends the known eastern dispersal of the Y-3 tephra to over 800 km from CF (Fig. 7) and would also imply that the area effected by ash deposition from this eruption is greater than 550,000 km$^2$, which was previously suggested by Caron et al. (2010). Importantly, the identification of the Y-3 at TP demonstrates the potential of this marker horizon to integrate the Italian and Aegean tephrostratigraphic records. This is significant as currently only two Italian tephra markers have been integrated within the Aegean tephrostratigraphic record, the P-11 (Pantelleria) and Campanian Ignimbrite/Y-5 layers (Sulpizio et al., 2010). Trace element glass chemistry verifies the correlation of TM-15 at Lago Grande di Monticchio (LGdM) to the Ionian Sea Y-3 tephra (Wulf et al., 2004). This eastern dispersal of the Y-3 eruption appears to be biased towards the intermediate and most evolved glass compositions (Fig. 6), while the southern dispersal (Ionian Sea) is dominated by the least and most evolved compositional end-members (Fig. 6).

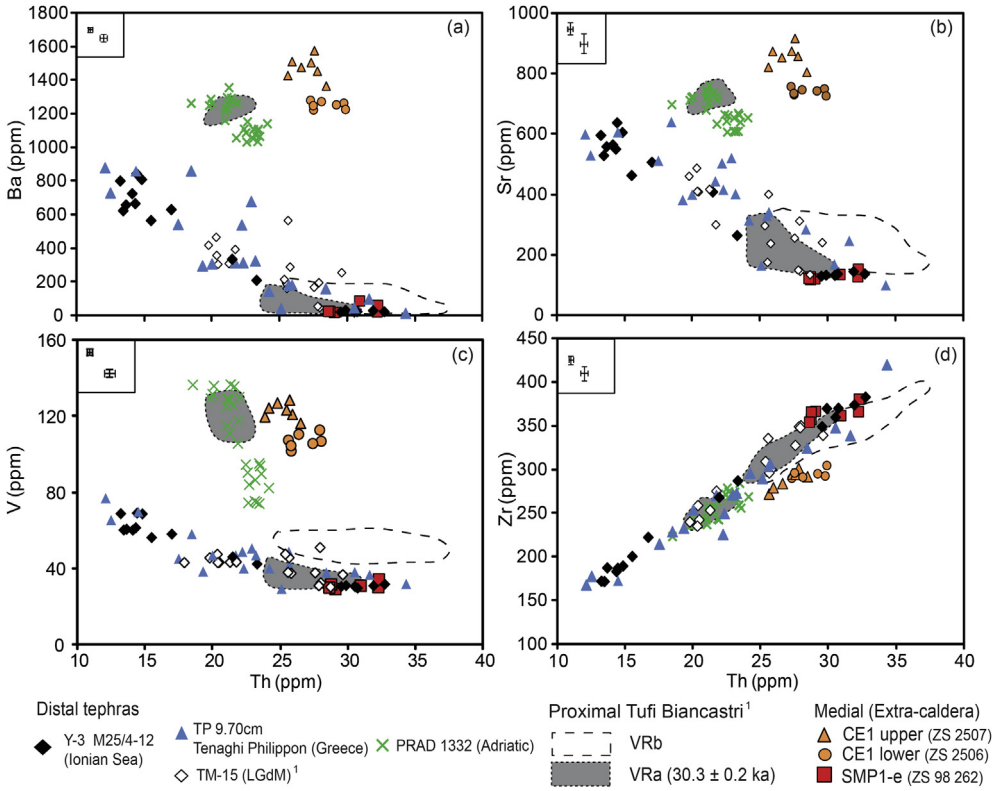


**Fig. 6.** Trace element glass compositions of the Ionian Sea Y-3 tephra (M25/4-12) compared to those of proximal intra-caldera Tufi Biancastri (Tomlinson et al., 2012) and extra-caldera deposits (SMP1-e, CE1; this study) from Campi Flegrei. The glass compositions of distal tephra layers TP 9.70, PRAD 1332 (this study), and LGdM TM-15 (Tomlinson et al., 2012). Error bars represents 2 standard deviations of repeat analyses of both the StHs6/-80G and ATHO-1G reference glasses.

Other proposed eastern occurrences of the Y-3 tephra recorded in the southern Adriatic (MD90-917 920; Zanchetta et al., 2008) and the Balkans (Fig. 1b) (Lake Ohrid; Wagner et al., 2008; Caron et al., 2010; Vogel et al., 2010; and Prespa; Damaschke et al., 2013) are supported by our new type locality Y-3 glass data. These tephra layers have major element glass compositions that match the diagnostic lower silica end-member of the Y-3 tephra, and also show similar compositional variability (Figs. 3 and 5). This verification indicates that the Y-3 tephra is a very important isochron for synchronising crucial terrestrial Mediterranean palaeoenvironmental records LGdM (Brauer et al., 2007), Lake Ohrid (Belmercheri et al., 2009; Lezine et al., 2010) and TP (Fletcher et al., 2010; Müller et al., 2011). This allows the synchronisation of records along an east-west transect extending from southern Italy via the Balkans to north-east Greece.

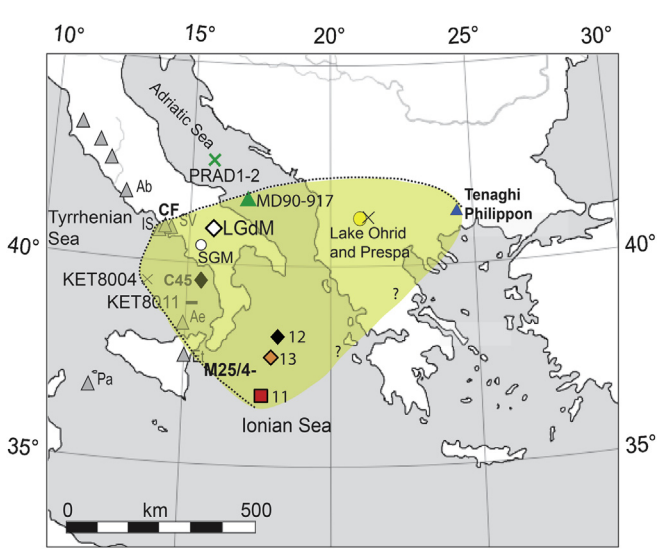


**Fig. 7.** The revised known dispersal and distribution of the Y-3 tephra.

The bi-modal K-trachytic cryptotephra PRAD 1332 recorded in the marine core PRAD 1-2, was previously correlated to TM-15, and by association, the Y-3 tephra and the VRa eruptive unit (Bourne et al., 2010). The VRa $^{40}Ar/^{39}Ar$ age was imported to the depth of PRAD 1332 (Bourne et al., 2010). Even though major and trace element glass data demonstrates that PRAD 1332 is not a correlative of the Y-3 tephra (Fig. 3, 5 and 6) the lower silica K-trachytic component of PRAD 1332 geochemically corresponds to the lower silica end-member of the VRa eruption. Consequently, a correlation with the VRa eruption might be argued, and thus the attribution of the $^{40}Ar/^{39}Ar$ age by Bourne et al. (2010) may still be considered sensible. Regardless of whether PRAD1332 is the distal equivalent of the VRa eruption, there are important implications associated with its erroneous correlation with the Y-3 tephra. Firstly, the stratigraphic position of PRAD 1332 close to the MIS 2/3 transition in PRAD1-2, is consistent with the position of Y-3 tephra in M25/4-12 (Negri et al., 1999), testifying to a high frequency of explosive activity at CF coinciding with this important environmental transition. Secondly, this reappraisal also currently limits the known north-easterly dispersal of the Y-3 tephra (Fig. 7).

Given that compositional variability is so diagnostic of the Ionian Sea Y-3 tephra, the absence of shard-specific glass data makes it more difficult to reliably assess other proposed correlations. Validating correlations with the Tyrrhenian Sea ash layers, the C-7 (Paterne et al., 1988; Zanchetta et al., 2008) and the A2/B2 (Munno and Petrosino, 2004) tephra deposits is challenging. Along

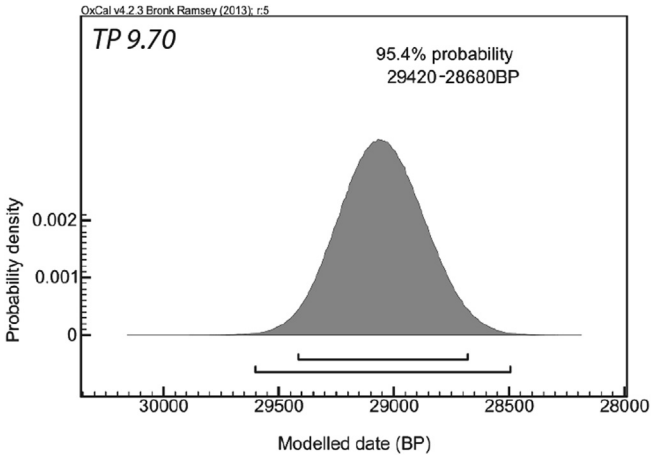


**Fig. 8.** Posterior probability density function generated for TP 9.70, the Tenaghi Philippon cryptotephra layer. The brackets at the base of the distribution represent the 95.4% and 99.7% probability ranges.

with the terrestrial S-19 tephra, from the San Gregorio Magno Basin (Munno and Petrosino, 2007), all these layers only demonstrate the presence of a higher silica K-trachytic glass component (Fig. 3a). Consequently, this glass data alone merely confirms that these layers derive from a Tufi Biancastri eruption but does not allow us to precisely verify an Y-3 tephra correlation.

### 5.2. Chronology of the Y-3 tephra

A Bayesian modelled age of 28,680–29,420 cal yrs BP has been obtained for the confirmed Y-3 tephra at Tenaghi Philippon (TP) (Fig. 8; = TP 9.70), based upon multiple radiocarbon ages from both above and below the tephra. Dated material includes mollusc shells, wood and bulk peat sediment, with the latter providing numerous ages above and below TP 9.70 (Müller et al., 2011). The '*Date*' function within OxCal was used to generate a robust age for the precise depth of the peak in shard concentrations (9.70 m), considered representative of the timing of deposition and the eruption (Fig. 9). Confidence in the robustness of the TP radiocarbon-based Bayesian age-model can be indirectly assessed via the accuracy of the modelled ages for other, previously correlated visible tephra layers within the TP-2005 sequence. This was done by removing the visible tephra ages from the model and comparing the modelled age for the tephra depth with the known published age of the tephra. TP 7.60 is correlated to the Cape Riva, Santorini and TP 12.87 to the Campanian Ignimbrite, CF (Müller et al., 2011). The age–depth model, with only the radiocarbon information included, produced modelled ages of 20,800–22,750 and 37,690–39,910 cal yrs BP, respectively, for these eruptions. This is in good agreement with available proximal ages for the Cape Riva (21,890–22,420 cal yrs BP; Lee et al., 2013; remodelled using IntCal13) and the CI eruption ($^{40}Ar/^{39}Ar$ 39,280 ± 110 yrs BP, De Vivo et al., 2001). Consequently, this demonstrates the integrity of the TP radiocarbon ages both above and below the Y-3 tephra.

The precise geochemical correlation between TP 9.70 and the Ionian Sea Y-3 tephra allow us to import the modelled age from TP to the Ionian Sea core M25/4-12 at a depth of 119.5 cm (b.s.f.). The imported TP 9.70 age (28,680–29,420 cal yrs BP) clearly provides a more precise chronological constraint than the previous (interpolated sapropel) age given to this tephra (Table 1). The TP 9.70 age also shows very good agreement with the calibrated $^{14}C$ age from directly above the OT0702-4/Y-3 layer in the Lake Ohrid record (28,780–29,980 cal yrs BP; Vogel et al., 2010). At LGdM the varve age of TM-15/Y-3 (25,900–28,620 yrs BP; Wulf et al., 2012) is slightly younger than the TP 9.70/Y-3 calibrated $^{14}C$ age. Independent ages for other tephras in this part of the LGdM stratigraphy have suggested that the varve chronology presents a slight underestimate of tephra ages (Brauer et al., 2000; Wulf et al., 2012).

Bronk Ramsey et al. (submitted for publication) use a Bayesian age–depth model to generate a marine reservoir corrected, integrated age for the A2/B2 Tyrrhenian Sea tephra layers that were previously correlated to the Ionian Sea Y-3 tephra (Munno and Petrosino, 2004). This yields a modelled age of 28,618–29,541 cal yrs BP, which is in perfect agreement with the TP 9.70/Y-3 age (28,680–29,420 cal yrs BP). Whilst available geochemical data from these two Tyrrhenian Sea layers (A2 and B2) is not sufficient to precisely validate their affinity to the Ionian Sea Y-3 tephra, this chronological agreement offers significant weight to the existing correlation. The $^{14}C$ age associated with the extra-caldera SMP1-e ignimbrite deposits (29,390–30,720 cal yrs BP)

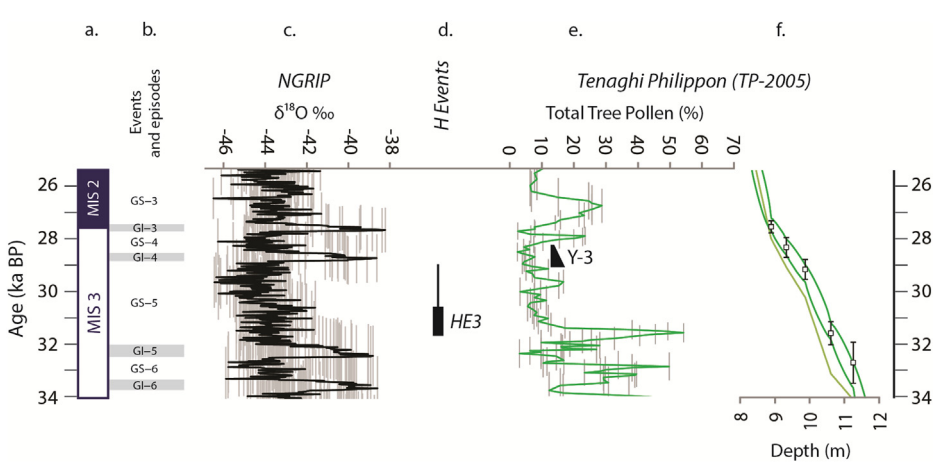


**Fig. 9.** Climatostratigraphic context of the Y-3 tephra at Tenaghi Philippon, NE Greece. Shown from left to right: (a) Marine Isotope Stage (Svensson et al., 2006, 2008); (b) The INTIMATE event stratigraphy (Lowe et al., 2008; Blockley et al., 2012). (c) The NGRIP oxygen isotope record based upon the GGIC05 timescale from Andersen et al. (2006) and Svensson et al. (2006). (d) Calibrated age ranges for Heinrich Event 3 from western European records (Bard et al., 2000; de Abreu et al., 2003) (thin line) and calculated ages (Thouveny et al., 2000) (black box). (e) Tenaghi Philippon (TP-2005) total tree pollen percentage curve and the stratigraphic position of the Y-3 cryptotephra. (f) The age–depth model (at 95.4% probability range) and radiocarbon ages on which it is based are also shown (green) alongside the original Müller et al. (2011) chronology (grey green line). Note all data have been adjusted to a yrs BP (1950) timescale. (For interpretation of the references to colour in this figure legend, the reader is referred to the web version of this article.)

on the Sorrentine Peninsula (Di Vito et al., 2008) is slightly older than the TP 9.70/Y-3 age. This age and the chemistry does not indicate the existing correlation between the SMP1-e ignimbrite deposits and the distal Ionian Sea Y-3 tephra is wrong (Zanchetta et al., 2008), but indicates further verification is required.

In terms of determining the absolute ordering of eruptive events at CF, the ages of the distal Y-3 (TP 9.70; 28,680–29,420 cal yrs BP) and the proximal VRa (29,900–30,700 $^{40}Ar/^{39}Ar$ yrs BP; Pappalardo et al., 1999) tephra would suggest that the former represents the younger of two closely spaced CF eruptions. In the central Adriatic marine core, PRAD1-2, the $^{14}C$ ages below the PRAD1332 cryptotephra layer provide a maximum age (Table 1) that would indicate that this eruption is younger than the eruption of the Y-3 tephra. Whilst geochemical evidence might point to a PRAD1332-VRa correlation, if accepted, their respective ages (Table 1) would suggest that dating either proximally or distally is erroneous. The negligible temporal gaps between the independent ages of the respective tephra deposits mean that validating the absolute ordering of these eruptive events will only be fully established through their identification in the same stratigraphic sequence. Owing to resurgent activity, intra-caldera deposits at CF are complex and consequently establishing the stratigraphic superposition of these eruptive events is more likely to be determined in the distal realm.

Where the diagnostic chemistry of the Ionian Sea Y-3 tephra underpins distal correlations, consistency between the TP 9.70/Y-3 (28680–29420 cal yrs BP; this study) and OT0702-4/Y-3 (28780–29980 cal yrs BP; Vogel et al., 2010) ages mean that they currently present the most reliable chronological constraints for the Y-3 tephra marker.

### 5.3. Climatostratigraphic context of the Y-3 tephra

The identification of the Y-3 tephra in the high-resolution TP palaeoenvironmental archive provides detailed information on the environmental conditions at the time of the Y-3 eruption. The Y-3 tephra at TP sits within the latter part of a period marked by a major reduction in tree pollen percentages (Fig. 9) that are related to stadial conditions (Müller et al., 2011). The age–depth model at TP suggests that the Y-3 tephra was deposited ~2300 years after the onset of stadial conditions. Within this overall period of reduced tree pollen percentages there is a small increase in total tree pollen percentages just below the Y-3 tephra which may reflect a brief climatic amelioration (Fig. 9). Comparisons between the TP and LGdM (Allen et al., 1999) palynological records using the Y-3 tephra marker (See Wutke et al., submitted for publication) reveals that the tephra occurs within the pollen zone correlated to Greenland Stadial 5 (GS-5) in both archives (Fletcher et al., 2010; Müller et al., 2011). The palaeoenvironmental record from Lake Ohrid, sequence JO2004 (Lezine et al., 2010), also suggests the Y-3 sits within a period of reduced total tree pollen. Combined evidence from these sites, in particular the very high resolution pollen stratigraphy from TP, suggest that the Y-3 tephra post-dates the onset of HS3 (*sensu* Sanchez Goni and Harrison, 2010) conditions in the Mediterranean region. The TP environmental record, on an independent time scale, suggests that the Y-3 eruption occurred during or after HE3 (Fig. 9), although given the inherent difficulties comparing marine and terrestrial radiocarbon datasets detection of the Y-3 within a high-resolution marine proxy record might be required to resolve this question. The independent dating evidence put forward for the Y-3 tephra herein strongly suggests that this eruption occurred sometime after the onset of Greenland Stadial 5 in the INTIMATE event stratigraphy (Blockley et al., 2012) and before the MIS 3/2 transition as defined by Svensson et al. (2006, 2008) (Fig. 9).

## 6. Conclusions

The Ionian Sea Y-3 tephra (M25/4-12) has a heterogeneous K-trachytic chemistry and glass compositions confirm a source from within the Campi Flegrei caldera. The combined major and trace element glass chemistry shows that the Y-3 tephra is not the distal equivalent of the proximal Tufi Biancastri VRa eruptive unit (30.3 ± 0.2 ka BP). None of the medial tephra investigated from extra-caldera localities fully satisfy the compositional range of the Ionian Sea Y-3 tephra and the precise proximal equivalent of this eruption remains unknown. The diagnostic glass chemistry of the Ionian Sea Y-3 tephra identified enables us to establish precise distal–distal tephra correlations. A correlative of the Ionian Sea Y-3 tephra is also preserved in the Tenaghi Philippon record, NE Greece, which markedly extends the eastern dispersal of this tephra. A Bayesian-based $^{14}C$ age depth-model for the Tenaghi Philippon record provides a robust age of 28,680–29,420 cal yrs BP for this distal marker tephra, which is in agreement with other distal age estimates. Previous work has shown that at Tenaghi Philippon the Y-3 marker tephra occurs in the later stages of a period linked to stadial conditions (Müller et al., 2011). Dating of the Y-3 would suggest that it was erupted after the onset of Greenland Stadial 5 and post-dates the beginning of Heinrich Stadial 3. Detailed geochemical characterisation and independent dating mean this widespread tephra layer offers both a crucial tephrostratigraphic and chronostratigraphic marker associated with an important climatic event.

## Acknowledgements

PGA was funded by the Reid Scholarship, Royal Holloway University of London and with support from the Central Research council, University of London. PGA, MH and ELT were also supported by the NERC RESET consortium (project number NE/E015905/1). JP acknowledges support through the German Research Foundation (DFG) and the Biodiversity and Climate Centre Frankfurt (BiK-F). This paper forms the RHOXTOR contribution 032. Thanks to Neil Holloway (Royal Holloway, University of London) for preparing samples in epoxy resin stubs ready for geochemical analysis. We would also like to the thank Siwan Davies and two anonymous reviewers for their detailed and helpful comments on an earlier version of this manuscript.

## Appendix A. Supplementary data

Supplementary data related to this article can be found at http://dx.doi.org/10.1016/j.quascirev.2014.04.002.

## References

Albert, P.G., Tomlinson, E.L., Smith, V.C., Di Roberto, A., Todman, A., Rosi, M., Marani, M., Muller, W., Menzies, M.A., 2012. Marine-continental tephra correlations: volcanic glass geochemistry from the Marsili Basin and the Aeolian Islands, Southern Tyrrhenian Sea, Italy. J. Volcanol. Geotherm. Res. 229–230, 74–94.

Aksu, A.E., Jenner, G., Hiscott, R.N., Isler, E.B., 2008. Occurrence, stratigraphy and geochemistry of Late Quaternary tephra layers in the Aegean Sea and the Marmara Sea. Mar. Geol. 252 (3–4), 174–192.

Allen, J.R.M., Brandt, U., Brauer, A., Hubberten, H., Huntley, B., Keller, J., Kraml, M., Mackerseb, A., Mingram, J., Negendank, J.F.W., Nowaczyk, N.R., Oberhansil, H., Watts, W.A., Wulf, S., Zolitschka, 1999. Rapid environmental changes in southern Europe during the last glacial period. Nature 400, 740–743.

Andersen, K.K., Svensson, A., Johnsen, S.J., Rasmussen, S.O., Bigler, M., Röthlisberger, R., Ruth, U., Siggaard-Andersen, M., Steffensen, J.P., Dahl-Jensen, D., Vinther, B.M., Clausen, H.B., 2006. Quat. Sci. Rev. 25 (23–24), 3246–3257.

Bard, E., Rostek, F., Turon, J., Gendreau, S., 2000. Hydrological impact of Heinrich events in the Subtropical North Atlantic. Science 289 (5483), 1321–1324.

Belmercheri, S., Namiotko, T., Roberts, C., von Granfenstein, U., Danielopol, D.L., 2009. Climate controlled ostracod preservation in Lake Ohrid (Albania, Macedonia). Palaeogeogr. Palaeoclimatol. Palaeoecol. 277, 236–245.
Blockley, S.P.E., Pyne-O'Donnell, S.D.F., Lowe, J.J., Matthews, I.P., Stone, A., Pollard, A.M., Turney, C.S.M., Molyneux, E.G., 2005. A new and less destructive laboratory procedure for the physical separation of distal glass tephra shards from sediments. Quat. Sci. Rev. 24, 1952–1960.
Blockley, S.P.E., Bronk Ramsey, C., Pyle, D.M., 2008a. Improved age modelling and high-precision age estimates of late Quaternary tephras, for accurate palaeoclimate reconstruction. J. Volcanol. Geotherm. Res. 177 (1), 251–262.
Blockley, S.P.E., Ramsey, C.B., Lane, C.S., Lotter, A.F., Blockley, S., 2008b. Improved age modelling approaches as exemplified by the revised chronology for the Central European varved lake Soppensee. Quat. Sci. Rev. 27 (1–2), 61–71.
Blockley, S.P.E., Lane, C.S., Hardiman, M., Rasmussen, S.O., Seierstad, I.K., Steffensen, J.P., Svensson, A., Lotter, A.F., Turney, C.S.M., Bronk Ramsey, C., INTIMATE members, 2012. Synchronisation of palaeoenvironmental records over the last 60,000 years, an extended INTIMATE group protocol. Quat. Sci. Rev. 36, 2–10.
Bourne, A., Lowe, J.J., Trincardi, F., Asioli, A., Blockley, S.P.E., Wulf, S., Matthews, I.P., Piva, A., Vigliotti, L., 2010. Distal tephra record for the last 105, 000 years from the core PRAD 1-2 in the Adriatic Sea: implications for marine tephrostratigraphy. Quat. Sci. Rev. 29 (23–24), 1–16.
Brauer, A., Mingram, J., Frank, U., Günter, C., Schettler, G., Wulf, S., Zolitschka, B., Negendank, J.F.W., 2000. Abrupt environmental oscillations during the Early Weichselian recorded at Lago Grande di Monticchio, southern Italy. Quat. Int. 73/74, 79–90.
Brauer, A., Allen, J.R.M., Mingram, J., Dulski, P., Wulf, S., Huntley, B., 2007. Evidence for last interglacial chronology and environmental change from Southern Europe. PNAS 104 (2), 450–455.
Bronk Ramsey, C., 2001. Development of the radiocarbon calibration program OxCal. Radiocarbon 43 (2), 355–363.
Bronk Ramsey, C., 2008. Deposition model for chronological records. Quat. Sci. Rev. 27 (1–2), 42–60.
Bronk Ramsey, C., Albert, P.G., Blockley, S.P.E., Hardiman, M., Housley, R.A., Lane, C.S., Lee, S., Matthews, I.P., Smith, V.C., Lowe, J., 2014. The chronology of the RESET tephra lattice. Quat. Sci. Rev. (submitted for publication).
Bronk Ramsey, C., 2009. Bayesian analysis of radiocarbon dates. Radiocarbon 51 (1), 337–360.
Buccheri, G., Bertoldo, G., Coppa, M.G., Munno, R., Pennetta, M., Siani, G., Valente, A., Vecchione, C., 2002a. Studio multidisciplinare della successione sedimentaria tardo-quaternaria proveniente dalla scarpata continentale del Golfo di Policastro (Tirreno meridionale). Boll. Soc. Geol. It. 121, 187–210.
Buccheri, G., Capretto, G., Di Donato, V., Esposito, P., Ferruzza, G., Pescatore, T., Russo Ermoli, E., Senatore, M.R., Sprovieri, M., Bertoldo, M., Carella, D., Madonia, G., 2002b. A high resolution record of the last deglaciation in the southern Tyrrhenian Sea: environmental and climatic evolution. Mar. Geol. 186, 447–470.
Calanchi, N., Cattaneo, A., Dinelli, E., Gasparotto, G., Lucchini, F., 1998. Tephra layers in Late Quaternary sediments of the central Adriatic Sea. Mar. Geol. 149, 191–209.
Caron, B., Sulpizio, R., Zanchetta, G., Siani, G., Santacroce, R., 2010. The Late Holocene to Pleistocene tephrostratigraphic record Lake Ohrid (Albania). C. R. Geosci. 342, 453–466.
Damaschke, M., Sulpizio, R., Zanchetta, G., Wagner, B., Böhm, A., Nowacyk, N., Rethemeyer, J., Hilgers, 2013. Tephrostratigraphic studies on a sediment core from Lake Prespa in the Balkans. Clim. Past 9, 267–287.
Dansgaard, W., Johnsen, S.J., Clausen, H.B., Dahljensen, D., Gundestrup, N.S., Hammer, C.U., Hvidberg, C.S., Steffensen, J.P., Sveinbjornsdottir, A.E., Jouzel, J., Bond, G., 1993. Evidence for general instability of past climate from a 250-kyr ice-core record. Nature 364, 218–220.
de Abreu, L., Shackleton, N.J., Schönfeld, J., Hall, M., Chapman, M., 2003. Millennial-scale oceanic climate variability off the Western Iberian margin during the last two glacial periods. Mar. Geol. 196 (1–2), 1–20.
De Vivo, B., Rolandi, G., Gans, P.B., Calvert, A., Bohrson, W.A., Spera, F.J., Belkin, H.E., 2001. New constraints on the pyroclastic eruptive history of the Campanian volcanic Plain (Italy). Mineral. Pet. 73, 47–65.
Di Vito, M.A., Sulpizio, R., Zanchetta, G., D'Orazio, M., 2008. The late Pleistocene pyroclastic deposits of the Campanian plain: new insights into the explosive activity of the Neapolitan volcanoes. J. Volcanol. Geotherm. Res. 177 (1), 19–48.
Fletcher, W.J., Sanchez-Goni, M.F., Allen, J.R.M., Cheddadi, R., Combourieu-Nebout, N., Huntley, B., Lawson, I., Londeix, L., Magri, D., Margari, V., Müller, U.C., Naughton, F., Novenko, E., Roucoux, K., Tzedakis, P.C., 2010. Millennial-scale variability during the last glacial in vegetation records from Europe. Quat. Sci. Rev. 29 (21–22), 2839–2864.
Hardiman, J.C., 1999. Deep sea tephra from Nisyros Island, eastern Aegean Sea, Greece. The Geological Society of London, Special Publication 166, pp. 69–88.
Hardiman, M., 2012. Testing and Refining the Chronology and Correlation of Mediterranean Pollen Records of Late Last Glacial Age using Tephrochronology (Unpublished Ph.D. thesis). University of London.
Jochum, K.P., Stoll, B., Herwig, K., Willbold, M., Hofmann, A.W., Amini, M., Aarburg, S., Abouchami, W., Hellebrand, E., Mocek, B., Raczek, I., Stracke, A., Alard, O., Bouman, C., Becker, S., Dücking, M., Brätz, H., Klemd, R., de Bruin, D., Canil, D., Cornell, D., de Hoog, C., Dalpé, C., Danyushevsky, L., Eisenhauer, A., Gao, Y., Snow, J.E., Groschopf, N., Günther, D., Latkoczy, C., Guillong, M., Hauri, E., Höfer, H.E., Lahaye, Y., Horz, K., Jacob, D.E., Kasemann, S.A., Kent, A.J.R., Ludwig, T., Zack, T., Mason, P.R.D., Meixner, A., Rosner, M., Misawa, K., Nash, B.P., Pfänder, J., Premo, W.R., Sun, W.D., Tiepolo, M., Vannucci, R., Vennemann, T., Wayne, D., Woodhead, J.D., 2006. MPI-DING reference glasses for in situ microanalysis: new reference values for element concentrations and isotope ratios. Geochem. Geophys. Geosyst. 7 (2).
Keller, J., Ryan, W.B.F., Ninkovich, D., Altherr, R., 1978. Explosive volcanic activity in the Mediterranean over the past 200,000 yr as recorded in deep-sea sediments. Geol. Soc. Am. Bull. 89, 591–604.
Keller, J., Kraml, M., Scheld, A., 1996. Late Quaternary tephrochronological correlation between deep-sea sediments and the land record in the Central Mediterranean. In: 30th International Geological Congress, Beijing, vol. 3, p. 204.
Kotthoff, U., Koutsodendris, A., Pross, J., Schmiedl, G., Bornemann, A., Marino, G., Peyron, O., Schiebel, R., 2011. Impact of Lateglacial cold events on the northern Aegean region reconstructed from marine and terrestrial proxy data. J. Quat. Sci. 26, 86–96.
Kraml, M., 1997. Laser $^{40}Ar/^{39}Ar$-Datierungen an distalen marinen Tephren desjungquartären mediterranen Vulkanismus (Ionisches Meer, METEOR-Fahrt 25/4) (Ph.D thesis). Albert-Ludwigs-Universität Freiburg, pp. 216.
Le Bas, M.J., Le Maitre, R.W., Streckeisen, A., Zanettin, B., 1986. A chemical classification of volcanic rocks based on the total alkali-silica diagram. J. Pet. 27, 745–750.
Lee, S., Bronk Ramsey, C., Hardiman, M., 2013. Modelling the age of the Cape Riva (Y-2) Tephra. Radiocarbon 55, 3–4.
Lezine, A.-M., von Grafenstein, U., Andrsen, N., Belmecheri, S., Bordon, A., Caron, B., Cazet, J.-P., Erlenkeuser, H., Fouache, E., Grenier, C., Huntsman-Mapila, P., Hureau-Mazaudier, D., Manelli, D., Mazaud, A., Robert, C., Sulpizio, R., Tiercelin, J.-J., Zanchetta, G., Zeqollari, Z., 2010. Lake Ohrid, Albania, provides an exceptional multi-proxy record of environmental changes during the last glacial-interglacial cycle. Palaeogeogr. Palaeoclimatol. Palaeoecol. 287, 116–127.
Lowe, J.J., Blockley, S.P.E., Trincardi, F., Asioli, A., Cattaneo, A., Matthews, I.P., Pollard, M., Wulf, S., 2007. Age modelling of late Quaternary marine sequences from the Adriatic: towards improved precision and accuracy using volcanic event stratigraphy. Cont. Shelf Res. 27, 560–582.
Lowe, J.J., Rasmussen, S.O., Bjorck, S., Hoek, W.Z., Steffensen, J.P., Walker, M.J.C., Yu, Z.C., 2008. Synchronisation of palaeoenvironmental events in the North Atlantic region during the Last Termination: a revised protocol recommended by the INTIMATE group. Quat. Sci. Rev. 27, 6–17.
Margari, V., Pyle, D.M., Bryant, C., Gibbard, P.L., 2007. Mediterranean tephra stratigraphy revisited: results from a long terrestrial sequence on Lesvos Island, Greece. J. Volcanol. Geotherm. Res. 163 (1–4), 34–54.
Müller, U.C., Pross, J., Tzedakis, P.C., Gamble, C., Kotthoff, U., Schniedl, G., Wulf, S., Christanis, K., 2011. The role of climate in the spread of modern humans into Europe. Quat. Sci. Rev. 30 (3–4), 273–279.
Munno, R., Petrosino, P., 2004. New constraints on the occurrence of Y-3 Upper Pleistocene tephra marker layer in the Tyrrhenian Sea. Il Quat. 17, 11–20.
Munno, R., Petrosino, P., 2007. The Late Quaternary tephrostratigraphical record of the San Gregorio Magno basin (southern Italy). J. Quat. Sci. 22 (3), 247–266.
Negri, A., Capotondi, L., Keller, J., 1999. Calcareous nannofossils, planktonic foraminifera and oxygen isotopes in the Late Quaternary Sapropels of the Ionian Sea. Mar. Geol. 157, 89–103.
North Greenland Ice Core Project Members, 2004. High-resolution record of Northern Hemisphere climate extending into the last interglacial period. Nature 431, 147–151.
Orsi, G., DeVita, S., Di Vito, M., 1996. The restless, resurgent, Campi Flegrei nested caldera (Italy): constraints on its evolution and configuration. J. Volcanol. Geotherm. Res. 74 (3–4), 179–214.
Pappalardo, L., Civetta, L., D'Antonio, M., Deino, A., Di Vito, M., Orsi, G., Carandente, A., De Vita, S., Isaia, R., Piochi, M., 1999. Chemical and Sr-isotopical evolution of the Phlegraean magmatic system before the Campanian Ignimbrite and Neapolitan Yellow Tuff eruptions. J. Volcanol. Geotherm. Res. 91 (2–4), 141–166.
Paterne, M., Guichard, F., Labeyrie, J., Gilliot, P.Y., Duplessy, J.C., 1986. Tyrrhenian Sea tephrochronology of the oxygen isotope record for the past 60,000 yrs. Mar. Geol. 72, 259–285.
Paterne, M., Guichard, F., Labeyrie, J., 1988. Explosive activity of the South Italian volcanoes during the past 80,000 years as determined by marine tephrochronology. J. Volcanol. Geotherm. Res. 34, 153–172.
Paterne, M., Guichard, F., Duplessy, J.C., Siani, G., Sulpizio, R., Labeyrie, J., 2008. A 90,000-200, 000 yrs marine tephra record of Italian volcanic activity in the Central Mediterranean Sea. J. Volcanol. Geotherm. Res. 177 (1), 187–196.
Piva, A., Asioli, A., Andersen, N., Grimalt, J.O., Schneider, R.R., Trincardi, F., 2008. Climatic cycles as expressed in sediments of the PROMESS1 borehole PRAD 1-2, central Adriatic, for the last 370 ka: 2. Paleoenvironmental evolution. Geochem. Geophys. Geosyst. 9 (3), 1–21.
Pross, J., Tzedakis, P.C., Christanis, K., Schmiedl, G., Hooghiemstra, H., Müller, U.C., Kotthoff, U., Milner, A., 2007. Tenaghi Philippon re-visited: drilling a continuous lower-latitude terrestrial climate archive of the last 250,000 years. Sci. Drill. 5, 30–32.
Pross, J., Kotthoff, U., Müller, U.C., Peyron, O., Dormoy, I., Schmiedl, G., Kalaitzidis, S., Smith, A.M., 2009. Massive perturbation in terrestrial ecosystems of the Eastern Mediterranean region associated with the 8.2 kyr BP climatic event. Geology 37, 887–890.
Ramrath, A., Zolitschka, B., Wulf, S., Negendank, F.W., 1999. Late Pleistocene climatic variations as recorded in two Italian maar lakes (Lago di Mezzano, Lago Grade di Monticchio). Quat. Sci. Rev. 18, 977–992.

Rasmussen, S.O., Andersen, K.K., Svensson, A.M., Steffensen, J.P., Vinther, B., Clausen, H.B., Siggaard-Andersen, M.L., Johnsen, S.J., Larsen, L.B., Dahl-Jensen, D., Bigler, M., Röthlisberger, R., Fischer, H., Goto-Azuma, K., Hansson, M., Ruth, U., 2006. A new Greenland ice core chronology for the last glacial termination. J. Geophys. Res. 111, D06102.

Reimer, P.J., Bard, E., Bayliss, A., Beck, J.W., Blackwell, P.G., Bronk Ramsey, C., Buck, C.E., Cheng, H., Edwards, R.L., Friedrich, M., Grootes, P.M., Guilderson, T.P., Haflidason, H., Hajdas, I., Hatté, C., Heaton, T.J., Hoffmann, D.L., Hogg, A.G., Hughen, K.A., Kaiser, K.F., Kromer, B., Manning, S.W., Niu, M., Reimer, R.W., Richards, D.A., Scott, E.M., Southon, J.R., Staff, R.A., Turney, C.S.M., van der Plicht, J., 2013. IntCal13 and Marine13 radiocarbon age calibration curves 0–50,000 years cal BP. Radiocarbon 55 (4), 1869–1887.

Sanchez Goñi, M.F., Turon, J.L., Eynaud, F., Gendreau, S., 2000. European climatic response to millenial-scale changes in the atmosphere-ocean system during the Last Glacial period. Quat. Res. 54, 394–403.

Sanchez Goni, M.F., Harrison, S.P., 2010. Millennial-scale climate variability and vegetation changes during the Last Glacial: concepts and terminology. Quat. Sci. Rev. 29, 2823–2827.

Schiano, P., Clocchiatti, R., Ottolini, L., Busa', T., 2001. Transition of Mount Etna lavas from a mantle-plume to an island-arc magmatic source. Nature 412, 900–904.

Schiano, P., Clocchiatti, R., Ottolini, L., Sbrana, A., 2004. The relationship between potassic, calc-alkaline and Na-alkaline magmatism in South Italy volcanoes: A melt inclusion approach. Earth Planet. Sci. Lett. 220, 121–137.

Siani, G., Paterne, M., Michel, E., Sulpizio, R., Sbrana, A., Arnold, M., Haddad, G., 2001. Mediterranean sea surface radiocarbon reservoir age changes since the last glacial maximum. Science 294, 1917.

Siani, G., Sulpizio, R., Paterne, M., Sbrana, A., 2004. Tephrostratigraphy study for the last 18,000 14C years in a deep-sea sediment sequence for the South Adriatic. Quat. Sci. Rev. 23, 2485–2500.

Smith, V.C., Isaia, R., Pearce, N.J.G., 2011. Tephrostratigraphy and glass compositions of post-15 kyr Campi Flegrei eruptions: implications for eruption history and chronostratigraphic markers. Quat. Sci. Rev. 30, 3638–3660.

Sulpizio, R., Zanchetta, G., Paterne, M., Siani, G., 2003. A review of tephrostratigraphy in central and southern Italy during the last 65 ka. Il Quat. 16, 91–108.

Sulpizio, R., Zanchetta, G., D'Orazio, M., Vogel, H., Wagner, B., 2010. Tephrostratigrapy and tephrochronology of lakes Ohrid and Prespa, Balkans. Biogeosciences 7, 3273–3288.

Svensson, A., Andersen, K.K., Bigler, M., Clausen, H.B., Dalh-jensen, Davies, S.M., Johnsen, S.J., Muscheler, R., Rasmussen, S.O., Röthlisberger, R., Steffensen, J.P., Vinther, B.M., 2006. The Greenland Ice Core Chronology 2005, 15-42 ka. Part 2: comparison to other records. Quat. Sci. Rev. 25 (23–24), 3258–3267.

Svensson, A., Andersen, K.K., Bigler, M., Clausen, H.B., Dahl-Jensen, D., Davies, S.M., Johnsen, S.J., Muscheler, R., Parrenin, F., Rasmussen, S.O., Röthlisberger, R., Seierstad, I.K., Steffensen, J.P., Vinther, B.M., 2008. A 60 000 year Greenland stratigraphic ice core chronology. Clim. Past 4, 47–57.

Thouveny, N., Moreno, E., Delanghe, D., Candon, L., Lancelot, Y., Shackleton, N.J., 2000. Rock magnetic detection of distal ice-rafted debris: clue for the identification of Heinrich layers on the Portuguese margin. Earth Planet. Sci. Lett. 180 (1–2), 61–75.

Tomlinson, E.L., Thordarson, T., Muller, W., Thirlwall, M., Menzies, M.A., 2010. Microanalysis of tephras by LA-ICP-MS-Strategies, advantages and limitations assessed using the Thorsmork ignimbrite (Southern Iceland). Chem. Geol. 279 (3–4), 73–89.

Tomlinson, E.L., Arienzo, I., Civetta, L., Wulf, S., Smith, V.C., Hardiman, M., Lane, C.S., Carandente, A., Orsi, G., Rosi, M., Muller, W., Thirwall, M.F., Menzies, M., 2012. Geochemistry of the Phlegraean Fields (Italy) proximal sources for major Mediterranean tephras: implications for the dispersal of Plinian and co-ignimbritic components of explosive eruptions. Geochim. Cosmochim. Acta 93, 102–128.

Tomlinson, E.L., Albert, P.G., Wulf, S., Civetta, L., Brown, R., Smith, V.C., Keller, J., Orsi, G., Bourne, A., Menzies, M.A., 2014. Tephras from Ischia: dating eruptions and geochemical changes. J. Volcanol. Geot. Res. (submitted for publication).

Tzedakis, P.C., Lawson, I.T., Frogley, M.R., Hewitt, G.M., Preece, R.C., 2002. Buffered tree population changes in a Quaternary refugium: evolutionary implications. Science 297, 2044–2047.

Tzedakis, P.C., Frogley, M.R., Lawson, I.T., Preece, R.C., Cacho, I., de Abreu, L., 2004. Ecological thresholds and patterns of millennial-scale climate variability: the response of vegetation in Greece during the last glacial period. Geology 32, 109–112.

Vezzoli, L., 1991. Tephra layers in the Bannock Basin (Eastern Mediterranean). Mar. Geol. 100, 21–34.

Vinci, A., 1985. Distribution and chemical composition of tephra layers from Eastern Mediterranean abyssal sediments. Mar. Geol. 64, 143–155.

Vogel, H., Zanchetta, G., Sulpizio, R., Wagner, B., Nowaczyk, N., 2010. A tephrostratigraphic record for the last glacial-interglacial cycle from Lake Ohrid, Albania and Macedonia. J. Quat. Sci. 25, 320–338.

Wagner, B., Sulpizio, R., Zanchetta, G., Wulf, Wessels, M., Daut, G., Nowaczyk, N., 2008. The last 40 ka tephrostratigraphic record of Lake Ohrid, Albania and Macedonia: a very distal archive for ash dispersal from Italian volcanoes. J. Volcanol. Geotherm. Res. 177 (1), 71–80.

Wulf, S., Kraml, M., Brauer, A., Keller, J., Negendank, J.F.W., 2004. Tephrochronology of the 100 ka lacustrine sediment record of Lago Grande di Monticchio (southern Italy). Quat. Int. 122, 7–30.

Wulf, S., Kraml, M., Keller, J., 2008. Towards a detailed distal tephrostratigraphy in the Central Mediterranean: the last 20,000 yrs record of Lago Grande di Monticchio. J. Volcanol. Geotherm. Res. 177, 118–132.

Wulf, S., Keller, J., Paterne, M., Mingram, J., Lauterbach, S., Opitz, S., Sottili, G., Giaccio, B., Albert, P.G., Satow, C., Tomlinson, E.L., Viccaro, M., Brauer, A., 2012. The 100-133 ka record of Italian explosive volcanism and revised tephrochronology of Lago Grande di Monticchio. Quat. Sci. Rev. 58, 104–123.

Wutke, K., Wulf, S., Tomlinson, E.L., Hardiman, M., Dulski, P., Luterbacher, J., Brauer, A., 2014. Geochemical properties and environmental impacts of seven Campanian tephra layers deposited between 40-38 ka BP in the varved lake sediments of Lago Grande di Monticchio, southern Italy. Quat. Sci. Rev. SI: Volcanic Ash Synchronisation. (submitted for publication).

Zanchetta, G., Sulpizio, R., Giaccio, B., Siani, G., Paterne, M., Wulf, S., D'Orazio, M., 2008. The Y-3 tephra: a last glacial stratigraphic marker for the central Mediterranean basin. J. Volcanol. Geotherm. Res. 177 (1), 145–154.

Please cite this article in press as: Albert, P.G., et al., Revisiting the Y-3 tephrostratigraphic marker: a new diagnostic glass geochemistry, age estimate, and details on its climatostratigraphical context, Quaternary Science Reviews (2014), http://dx.doi.org/10.1016/j.quascirev.2014.04.002